NASA
Technical
Paper
2177

September 1983

Development of a Distributed-Parameter Mathematical Model for Simulation of Cryogenic Wind Tunnels

John S. Tripp

NASA

25th Anniversary
1958-1983

NASA
Technical
Paper
2177

1983

Development of a Distributed-Parameter Mathematical Model for Simulation of Cryogenic Wind Tunnels

John S. Tripp
Langley Research Center
Hampton, Virginia

NASA
National Aeronautics
and Space Administration

**Scientific and Technical
Information Branch**

CONTENTS

INTRODUCTION

Cryogenic wind tunnels have become important tools for high Reynolds number research. (See ref. 1 by Kilgore et al.) A cryogenic wind tunnel (T'2) has been built at the Toulouse Research Center, Toulouse, France. (See ref. 2 by Blanchard, Dor, and Breil.) The 0.3-Meter Transonic Cryogenic Tunnel (0.3-m TCT), built as a pilot facility, is at the Langley Research Center. The National Transonic Facility (NTF) at the Langley Research Center (see ref. 3 by Fuller), which is expected to become operational in 1983, is a closed-circuit, fan-driven, continuous-flow, pressurized cryogenic tunnel operating at pressures up to 9 atm (1 atm = 101.1 kPa) and having a 6.25-m^2-area slotted test section that is 7.6 m in length. The facility will operate at temperatures ranging from ambient down to about 100 K. Liquid nitrogen (LN_2) sprayed into the tunnel upstream from the fan nacelle performs three cryogenic-cooling functions: (1) initial cooldown, (2) steady-flow temperature regulation by balancing the energy added by the fan, and (3) primary temperature control in passing from one steady-flow condition to another. Total-pressure control is accomplished by venting tunnel gaseous nitrogen (GN_2) to the atmosphere. Both LN_2 and GN_2 flows are regulated by means of servo-control valves. Fan-motor speed determines coarse Mach number variation, whereas fan inlet guide vanes furnish fine vernier Mach number variation. The tunnel shell has interior thermal insulation with an aluminum inner liner. This limits atmospheric-heat penetration to a negligible amount and reduces energy consumption. See figure 1 for a schematic diagram of the NTF.

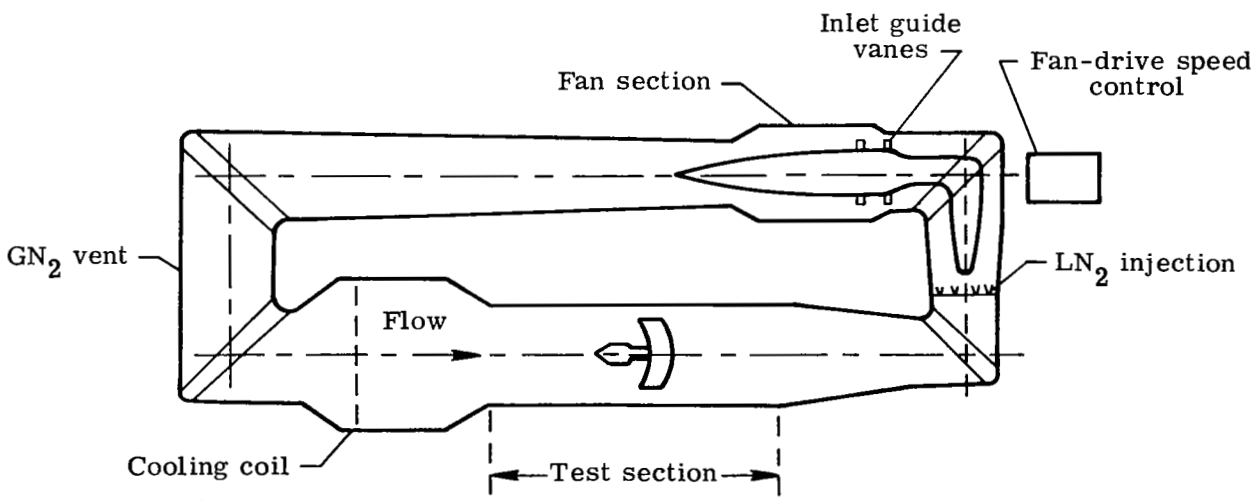

Figure 1.- Schematic diagram of the National Transonic Facility (NTF).

The high cost of liquid nitrogen makes efficient operation of a cryogenic tunnel important. In order to minimize operating cost, it is necessary that such a facility be equipped with automatic controls which perform the following functions:

(1) Maintain steady flow at the most efficient setting during test dwell.

(2) Drive the system along the most efficient transition path from one steady-flow setting to the next as quickly as possible.

Modern control-system synthesis techniques require that the dynamic process to be controlled be modeled analytically either in a discrete formulation as a system of difference equations or in a continuous formulation as a system of differential equations in state variable form. The thermodynamic and fluid-dynamic processes in the wind tunnel are described by the three-dimensional Navier-Stokes equations which require numerical solution. The complexity of this three-dimensional formulation is beyond the scope of modern distributed-parameter control synthesis techniques, and numerical solution of the equations requires lengthy, expensive computation. Consequently, the control-system designer must resort to a simplified approach, such as segmentation of the process into a set of lumped parameter stations which may then be treated as a high-order multivariable system with time delays. Because the accuracy of such an approximation is limited, a need exists for a dynamic model whose accuracy is adequate for control-system design and performance evaluation, but whose numerical solution will execute on a digital computer at reasonable speed and cost. The one-dimensional distributed-parameter dynamic model described herein is intended to satisfy this need.

SYMBOLS

A_R	diffuser area ratio
A_S	projected-strut frontal area, m^2
A_T	test-section cross-sectional area at throat, m^2
a	local speed of sound, m/sec
B	body force vector in three-dimensional space, N
b	$= \frac{\gamma - 1}{2\gamma}$ (see eq. (A14))
C_D	drag coefficient
C_{DMX}	variable model-blockage flow coefficient
C_f	flow coefficient for reentry mass flow
C_{ORF}	slot (plenum test-section) pressure-difference flow coefficient, $kg\text{-}m^2/N\text{-}sec$
C_R	heat-transfer correction factor
C_T^k	variable defined in equation (93)
C_X	artificial-viscosity coefficient
C_{XM}	boundary-layer flow coefficient
c_M	specific heat of metal liner, kJ/kg-K
c_p	specific heat of gas at constant pressure, kJ/kg-K

c_v	specific heat of gas at constant volume, kJ/kg-K
$D^k_{V,n}$	vector difference defined in equation (95)
d	tube diameter, m
$d^k_{u,n}$	difference defined in equation (94)
E_{PL}	plenum internal energy, kJ
e	internal energy, kJ/kg
F	vector defined in equation (76)
F_S	surface force vector in three-dimensional space, N
f	function
G	vector-function relation of fan
GN_2	gaseous nitrogen
H	vector defined in equation (77)
h	enthalpy, kJ/kg
h_N	total enthalpy of LN_2, kJ/kg
j'	momentum-flow rate per unit length, kg/sec
K	diffuser loss factor
K_H	diffuser correction factor defined in equation (37)
K_δ	constant defined in equation (45)
k	thermal conductivity of gas, kJ-m/K-sec
k_H	diffuser correction factor defined in equation (34)
L	length, m
LN_2	liquid nitrogen
M	Mach number
m	mass, kg
m'	mass-flow rate per unit length, kg/m-sec
N	number of quantized stations
N_{Pr}	Prandtl number
N_{Re}	Reynolds number

$P^k_{V,n}$	vector defined in equation (96)
p	static pressure, atm (1 atm = 101.1 kPa)
p'_t	corrected total pressure
Q	external heat flow into control volume, kJ
q	heat-flow rate, kJ/sec
q'	heat-flow rate per unit length, kJ/m-sec
q'_S	heat transfer from liner, kJ/m-sec
R	gas constant, kJ/kg-K
R_D	constant defined in equation (23)
R_W	wall resistance, km^3/kJ
R_1	diffuser-inlet equivalent radius, m
r_F	fan compression ratio
r_H	diffuser pressure ratio defined in equation (33)
r'_H	corrected diffuser pressure ratio
S	surface vector in three-dimensional space, m^2
s	entropy, kJ/K
T	gas temperature, K
T_M	liner temperature, K
t	time, sec
t_M	liner thickness, m
U	velocity vector
U_T	heat-transfer coefficient, kJ/km^3
U^k_n	artificial-viscosity vector
u	velocity, m/sec
V	state vector defined in equation (73)
V^k_n	value of state vector V at station x_n and time t_k
v	specific volume, m^3/kg
υ	volume, m^3

W	external work done by control volume, kJ
w	mass-flow rate, kg/sec
w_B	boundary-layer component of slot-flow rate, kg/sec
w_{DM}	model-blockage component of slot-flow rate, kg/sec
w_f	extracted component of reentry mass-flow rate, kg/sec
w_G	GN_2-vent flow rate, kg/sec
w_N	LN_2-injection flow rate, kg/sec
w_{SS}	supersonic component of slot-flow rate, kg/sec
w_{TH}	average test-section mass-flow rate, kg/sec
x	spatial coordinate, m
α	inlet-guide-vane position, deg
γ	ratio of specific heats
Δ	differencing increment
δ	increment used in equations (33) and (39)
δ^*	boundary-layer displacement thickness, m
ε	increment used in equations (38) and (39)
η_F	fan efficiency
2θ	total diffuser expansion angle, rad
θ_1	boundary-layer momentum thickness, m
μ	coefficient of viscosity, N-sec/m^2
ν	fan speed, rpm
ρ	density, kg/m^3
ρ_M	liner density, kg/m^3
σ	normal stress, N/m^2
ω	cross-sectional area, m^2

Subscripts:

DM	model blockage
E	slot exit (plenum test section)

EX	test-section exit
F	fan outlet
G	GN_2 (gaseous nitrogen)
N	LN_2 (liquid nitrogen); tunnel outlet, for example, in equation (74)
ORF	plenum test section
PL	plenum
R	flow loss
RE	reentry
s	smoothing
TS	test section
t	total value
xx	x-component of stress of force

Superscripts:

-	average value
~	predicted value
^	corrected value

Special symbol:

∇	vector del operator

A dot over a symbol denotes a derivative with respect to time.

DEVELOPMENT OF ONE-DIMENSIONAL MODEL

General Assumptions

The wind tunnel is modeled as a one-dimensional tube of varying cross-sectional area, in which the flow is assumed to be uniform across every cross section. Consequently, rotational effects and mixing caused by turns in the tunnel are neglected. In addition, longitudinal mixing caused by diffusion and turbulence is not modeled. Although viscous shearing stresses are neglected, frictional momentum losses at the walls are included.

Thermodynamic properties are computed by means of ideal-gas laws. Real-gas effects, important at low temperatures, could be readily included. Heat transfer is assumed to occur only between the gas and the tunnel inner liner; heat penetration from the outer shell through the insulation to the liner is neglected. Liquid-

nitrogen evaporative effects on total pressure, which are observed primarily at the lowest temperatures, have not been considered.

The tunnel fan is represented as an algebraic functional relationship with no inherent flow dynamics. Thus, the fan model is instantaneous, exhibiting no time delay. Inlet-guide-vane actuator dynamics are included. The fan model determines the functional relationships between tunnel inlet and outlet flows, which effectively closes the tunnel circuit.

The plenum is modeled as a lumped volume attached to the distributed test section. All external processes, including actuators and automatic controllers, are modeled as lumped-parameter dynamical systems. The numerical solution of the set of ordinary differential equations which describe the lumped-parameter processes is synchronized in time with the numerical solution of the partial differential equations of flow. This synchronized combination of one- and two-dimensional systems is well-suited for the CDC[1] CYBER 203 vector-processing digital computer (ref. 4) on which the solutions are obtained.

Derivation of One-Dimensional Flow Equations

The three-dimensional equations of fluid flow in integral form are applied to a differential element of a one-dimensional tube of varying cross-sectional area in order to derive a one-dimensional system of partial differential equations analogous to the three-dimensional Navier-Stokes equations. The three basic conservation laws, expressed in vector notation (ref. 5), are given as follows:

(1) Continuity:

$$\int_S \rho U \cdot dS + \frac{\partial}{\partial t} \int_\nu \rho \, d\nu = 0 \tag{1}$$

(2) Linear momentum:

$$\int_S \rho U \, U \cdot dS + \frac{\partial}{\partial t} \int_\nu \rho U \, d\nu = F_S + \int_\nu B \, d\nu \tag{2}$$

(3) Energy:

$$\int_S \left(e_t + \frac{p}{\rho}\right) \rho U \cdot dS + \frac{\partial}{\partial t} \int_\nu e_t \rho \, d\nu = \frac{dQ}{dt} - \frac{dW}{dt} \tag{3}$$

where

ρ density of gas

U velocity vector of mass flow

[1]CDC: Registered trademark of Control Data Corporation.

S	surface vector of volume
ν	volume
F_S	surface force vector
B	body force vector
p	static pressure
e_t	total internal energy of gas
Q	external heat flow into control volume
W	external work done by control volume

By referring to figure 2, consider an incremental element of tube of length Δx with flow entering at x_1 and exiting at x_2.

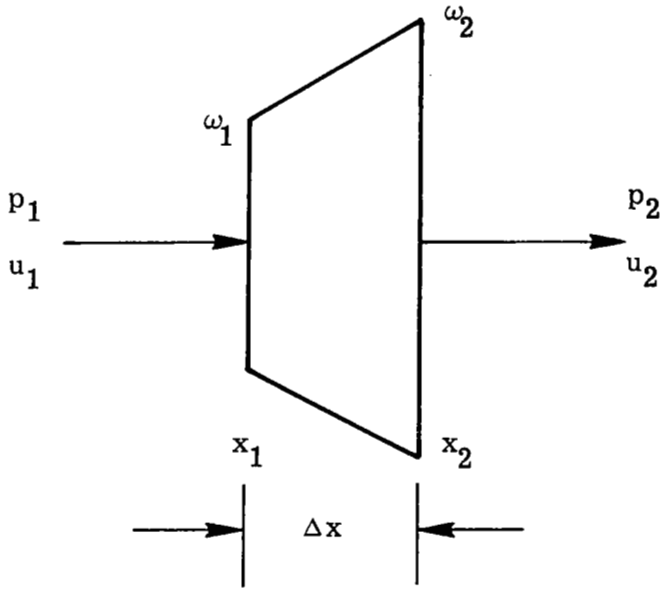

Figure 2.- Elemental flow volume ν.

The inviscid one-dimensional form of equations (1), (2), and (3) (ref. 6) is, respectively,

$$\frac{\partial}{\partial t}(\rho\omega) + \frac{\partial}{\partial x}(\rho u\omega) = 0 \tag{4}$$

$$\frac{\partial}{\partial t}(\rho u\omega) + \frac{\partial}{\partial x}(\rho u^2\omega + p\omega) = p\frac{d\omega}{dx} \tag{5}$$

and

$$\frac{\partial}{\partial t}(e_t \rho\omega) + \frac{\partial}{\partial x}(e_t \rho u\omega + pu\omega) = 0 \tag{6}$$

where ω is the cross-sectional area of the tube and u is stream velocity.

Equations (4), (5), and (6) are augmented to account for external mass, momentum, and heat transfer, respectively, into the element of volume. Let m', j', and q' denote mass-flow rate, momentum-flow rate, and heat-flow rate per unit length, respectively, into the element of volume. The surface integral in equation (1) for conservation of mass with mass flow into the element of volume becomes

$$\int_S \rho u \cdot dS = \frac{\partial(\rho u\omega)}{\partial x} \Delta x - m' \Delta x \tag{7}$$

so that equation (4) becomes

$$\frac{\partial}{\partial t}(\rho\omega) + \frac{\partial}{\partial x}(\rho u\omega) = m' \tag{8}$$

Similarly, the addition of momentum flow $j' \Delta x$ and heat flow $q' \Delta x$ into the element of volume results, respectively, in the equation for conservation of momentum

$$\frac{\partial}{\partial t}(\rho u\omega) + \frac{\partial}{\partial x}(\rho u^2\omega + p\omega) = p \frac{d\omega}{dx} + j' \tag{9}$$

and in the equation for conservation of energy

$$\frac{\partial}{\partial t}(e_t \rho\omega) + \frac{\partial}{\partial x}(e_t \rho u\omega + pu\omega) = q' \tag{10}$$

Equations (8), (9), and (10) are in the form employed by Carrière (ref. 7) in a dynamic analysis of an injector-driven wind tunnel that was solved by means of the method of characteristics.

In the present study, it is desired to account for heat transfer within the gas due to gas thermal conductivity. From Fourier's law of heat conduction, it follows that the rate of heat transfer through surface S into volume υ is

$$\left.\frac{dQ}{dt}\right|_k = -\int_S k \nabla T \cdot dS \tag{11}$$

where k is the thermal conductivity and $|_k$ denotes the component of heat transfer due to gas thermal conductivity. Because gas-to-gas heat transfer does not occur

along the outer surface of the surface integral, equation (11) is evaluated only at surfaces ω_1 and ω_2 (fig. 2) so that

$$\left.\frac{dQ}{dt}\right|_k = k\omega_2 \frac{\partial T}{\partial x} - k\omega_1 \frac{\partial T}{\partial x} = \frac{\partial}{\partial x}\left(k\omega \frac{\partial T}{\partial x}\right) \Delta x \tag{12}$$

The equation for conservation of energy (eq. (10)) then becomes

$$\frac{\partial}{\partial x}\left(e_t \rho u\omega + pu\omega - k\omega \frac{\partial T}{\partial x}\right) + \frac{\partial}{\partial t}(e_t \rho \omega) = q' \tag{13}$$

In this analysis, it is desired to consider the effects of fluid viscosity. The normal stress σ_{xx} for one-dimensional flow is (ref. 8)

$$\sigma_{xx} = \frac{4}{3} \mu \frac{\partial u}{\partial x} \tag{14}$$

where μ is the coefficient of viscosity. In the present one-dimensional approximation, shearing stresses are neglected. The surface force F_{xx} at points x_1 and x_2 (see fig. 2) due to normal viscous forces is of the form

$$F_{xx} = \omega \sigma_{xx} = \frac{4}{3} \mu \frac{\partial u}{\partial x} \omega \tag{15}$$

Consequently, the equation for conservation of momentum (eq. (9)) then becomes

$$\frac{\partial}{\partial t}(\rho u\omega) + \frac{\partial}{\partial x}\left(\rho u^2 \omega + p\omega - \frac{4}{3} \mu\omega \frac{\partial u}{\partial x}\right) = p \frac{d\omega}{dx} + j' \tag{16}$$

Empirical momentum losses obtained from data reported by Rao (ref. 9) will be introduced through the j' term.

The rate of flow work done at surfaces ω_1 and ω_2 by the normal force F_{xx} in equation (15) is

$$\left.\frac{dW_{xx}}{dt}\right|_w = F_{xx} \cdot U|_w = \frac{4}{3} \mu u\omega \frac{\partial u}{\partial x} \tag{17}$$

The energy equation for viscous flow with heat addition and thermal conduction is

$$\frac{\partial}{\partial x}\left(e_t \rho u\omega + pu\omega - k\omega \frac{\partial T}{\partial x} - \frac{4}{3} \mu u\omega \frac{\partial u}{\partial x}\right) + \frac{\partial}{\partial t}(e_t \rho \omega) = q' \tag{18}$$

Equations (8), (16), and (18) comprise the complete one-dimensional partial differential equations of flow that approximate the three-dimensional Navier-Stokes equations.

Heat Transfer Between Gas and Tunnel Wall

The one-dimensional time-dependent equations of flow developed in the preceding section include gas-to-gas heat-transfer effects. It will be found that heat transfer between the gas and the shell of the tube, corresponding to the wind-tunnel metal liner, is of primary importance. Let the rate of heat transfer from the liner to the gas (in joules per second per unit length) be denoted by q'_S, the metal temperature by T_M, the gas temperature by T, and the heat-transfer coefficient by U_T. For an annulus of tube of diameter d, the heat-transfer rate is

$$q'_S \equiv \pi d(T_M - T)U_T \tag{19}$$

An empirical relationship for U_T given by McAdams (ref. 10) is

$$\frac{1}{U_T} = \frac{1}{0.026 \frac{k}{d} N_{Re}^{0.8} N_{Pr}^{0.4}} + R_W \tag{20}$$

where

k thermal conductivity of gas

N_{Re} Reynolds number

N_{Pr} Prandtl number

R_W wall resistance

It has been found that a heat-transfer correction factor C_R is necessary to account for the additional surface area in the nacelle and turning-vane sections. The factor is employed as a multiplier so that equation (19) becomes

$$q'_S = \pi d(T_M - T)U_T C_R \tag{21}$$

Consider next the tunnel inner-liner temperature dynamics. Heat transfer from the liner to the gas occurs in accordance with equation (21). Lateral heat transfer within the liner from warmer to cooler regions is neglected. Consequently, the rate of change of the liner temperature $\dot{T}_M$ is

$$\dot{T}_M = \frac{(T - T_M)U_T}{c_M R_D} \tag{22}$$

where c_M is the specific heat of the liner material and

$$R_D = \rho_M t_M \tag{23}$$

where ρ_M is the liner density and t_M is the liner thickness. Equation (22) is employed as the governing equation for T_M.

ESTIMATION OF FLOW LOSSES

Introduction of Losses Into Equations of Flow

In the one-dimensional equations of flow, the viscous shear effects at the tunnel walls are neglected. However, frictional effects, especially in the test section and diffuser section of the wind tunnel, are significant and must be accounted for. According to Rao (ref. 9), nearly 60 percent of the total aerodynamic loss at Mach 1 occurs in these two sections. Since, of course, energy is conserved in the test section and diffuser, the "total energy loss" to which Rao refers is a loss in available energy, which is manifested as an increase in entropy. The entropy gradient at steady flow ds/dx, obtained in the appendix in equation (A23), is given by

$$\frac{ds}{dx} = \frac{R}{\omega u p}\left[\left(\frac{u^2}{2} - h\right)m' - uj' + q'\right] > 0 \tag{24}$$

Because of the assumption that the tunnel liner is perfectly insulated, external heat transfer q' equals zero for steady flow. Furthermore, mass transfer term m' is zero everywhere except for GN_2 and LN_2 transfer. Therefore, the increase in entropy must be due entirely to a momentum loss j' so that

$$j' < 0 \tag{25}$$

The steady-flow expression for the gradient of total pressure given in equation (A18) is

$$\frac{dp_t}{dx} = \frac{1}{\omega}\left(1 + \frac{\gamma - 1}{2}M^2\right)^{\frac{\gamma}{\gamma-1}} j' - \frac{1}{2\omega}\left(1 + \frac{\gamma - 1}{2}M^2\right)^{\frac{1}{\gamma-1}}\left[um' + (\gamma - 1)M^2\left(q' + \frac{1}{2}u^2 m'\right)\right] \tag{26}$$

With m' and q' both zero, equation (26) becomes

$$\frac{dp_t}{dx} = \frac{1}{\omega}\left(1 + \frac{\gamma - 1}{2}M^2\right)^{\frac{\gamma}{\gamma-1}} j' \tag{27}$$

and because j' is negative, dp_t/dx is negative. Rao (ref. 9) furnishes empirical relations for determination of total-pressure losses in the test section, in diffuser sections, at turning vanes, at cooling coils, and in the strut section of the NTF wind tunnel. With Rao's relations, dp_t/dx can be determined, and j' may be obtained from equation (27) for each of the tunnel sections as

$$j' = \omega\left(1 + \frac{\gamma - 1}{2} M^2\right)^{\frac{\gamma}{1-\gamma}}\left(\frac{dp_t}{dx}\right)_R \tag{28}$$

where $(dp_t/dx)_R$ is the total-pressure gradient due to flow losses obtained from Rao's relations. This value of j' is entered into the dynamic equations for unsteady flow, and dynamic effects in j' are neglected.

Calculation of Diffuser Losses

Total-pressure loss Δp_t along the length of a diffuser is given empirically by the equation (ref. 9)

$$\Delta p_t \equiv p_{t,2} - p_{t,1} = K\left(1 - \frac{1}{A_R}\right)^2 (p_{t,1} - p_1) \tag{29}$$

where

A_R diffuser area ratio

K diffuser loss factor

$p_{t,1}$ total pressure at inlet

p_1 static pressure at inlet

$p_{t,2}$ total pressure at outlet

Studies by Rao (ref. 9) and Henry et al. (ref. 11) show that for values of total diffuser expansion angle 2θ lying between 4° and 10°, the diffuser loss factor K depends on the ratio of the inlet boundary-layer displacement thickness δ^* and the diffuser-inlet equivalent radius R_1. For values of δ^*/R_1 less than 0.030, K is well approximated by the relationship

$$K = 0.075 + 5.88\,\frac{\delta^*}{R_1} \tag{30}$$

Substitution of equation (30) into equation (29) gives

$$\Delta p_t = (p_{t,1} - p_1)\left(1 - \frac{1}{A_R}\right)^2\left(0.075 + 5.88\,\frac{\delta^*}{R_1}\right) \tag{31}$$

Figure 3 shows a comparison of the diffuser pressure ratio

$$r_H = p_{t,1}/p_{t,2} \tag{32}$$

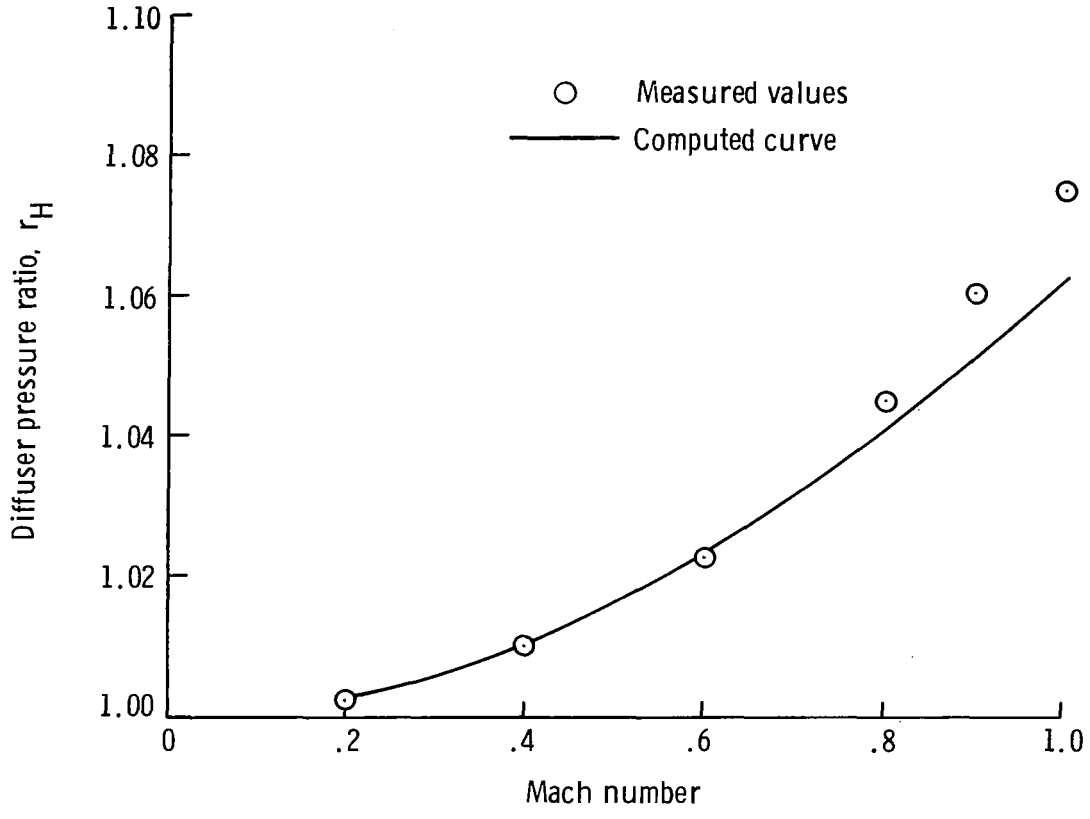

Figure 3.- Comparison of computed and measured diffuser pressure loss in the Langley 0.3-Meter Transonic Cryogenic Tunnel.

computed by using equation (31), with experimental values obtained by Rao (ref. 9) in the Langley 0.3-Meter Transonic Cryogenic Tunnel over the Mach number range from 0.2 to 1.0. Agreement is good up to a Mach number of 0.8, above which the computed values of r_H are too small. The ratio r_H, being nearly equal to 1.0, may be expressed by

$$r_H = 1 + \delta \tag{33}$$

where δ is a small increment and $0 < \delta \leq 0.061$, as computed from the experimental data. Because the values of r_H computed by equation (32) are too small, a correction factor to be applied to r_H can be defined as

$$k_H = p_{t,2}/p'_{t,2} \tag{34}$$

where $p'_{t,2}$ is the corrected value of $p_{t,2}$, thus giving a corrected diffuser pressure ratio

$$r'_H = k_H r_H = p_{t,1}/p'_{t,2} \tag{35}$$

The corrected pressure difference can be expressed as

$$\Delta p'_t = p'_{t,2} - p_{t,1} \tag{36}$$

The ratio of $\Delta p'_t$ to Δp_t defines a correction factor K_H. From equations (29), (32), (35), and (36), it follows that

$$K_H \equiv \frac{\Delta p'_t}{\Delta p_t} = \frac{p'_{t,2} - p_{t,1}}{p_{t,2} - p_{t,1}} = \frac{(1/r'_H) - 1}{(1/r_H) - 1} = 1 + \frac{1 - (1/k_H)}{r_H - 1} \tag{37}$$

Because k_H is slightly greater than 1, let

$$\frac{1}{k_H} = 1 - \varepsilon \tag{38}$$

Substituting equations (33) and (38) into (37) gives

$$\frac{\Delta p'_t}{\Delta p_t} = 1 + \frac{\varepsilon}{\delta} \equiv K_H \tag{39}$$

for values of $M > 0.6$. Correction factor K_H equals 1.0 for $M < 0.6$. The computations of ε, δ, and K_H from the data of figure 3 are summarized in table I. A second-degree polynomial, fit to the values of K_H obtained as a function of M for $M > 0.6$, is

$$K_H \approx 1.0 + 1.375(M - 0.6)^2 \tag{40}$$

TABLE I.- CORRECTION FACTOR OF DIFFUSER PRESSURE RATIO

M	r_H	δ	k_H	ε	$K_H \approx 1.0 + (\varepsilon/\delta)$	$K_H \approx 1.0 + 1.375(M - 0.6)^2$
0.6	1.025	0.025	1.0	0	1.00	1.00
.8	1.042	.042	1.0029	.0029	1.07	1.06
.9	1.052	.052	1.0076	.0076	1.15	1.12
1.0	1.061	.061	1.0132	.0132	1.22	1.22

which is tabulated in the final column of table I. Thus, p_t' is computed empirically by the relation obtained from equations (31), (36), and (37) as

$$\Delta p_t' = K_H p_1 \left[\left(1 + \frac{\gamma - 1}{2} M^2 \right)^{\frac{\gamma}{\gamma-1}} - 1 \right] \left(1 - \frac{1}{A_R} \right)^2 \left(0.075 + 5.88 \frac{\delta^*}{R_1} \right) \tag{41}$$

where K_H is obtained from equation (40).

The value of δ^*/R_1 is required as a function of Mach number M and Reynolds number N_{Re}. Shapiro (ref. 12) obtains δ^*/θ_1 as a function of M where θ_1 is defined as the momentum thickness of the boundary layer entering the diffuser. A curve of δ^*/θ_1 as a function of M, denoted by $f_2(M)$, is shown in figure 4 for values of M lying between 0 and 1.2. Rao (ref. 9) estimates θ_1 by the relation

$$\theta_1 = \frac{L_{TS}}{2} C_D \tag{42}$$

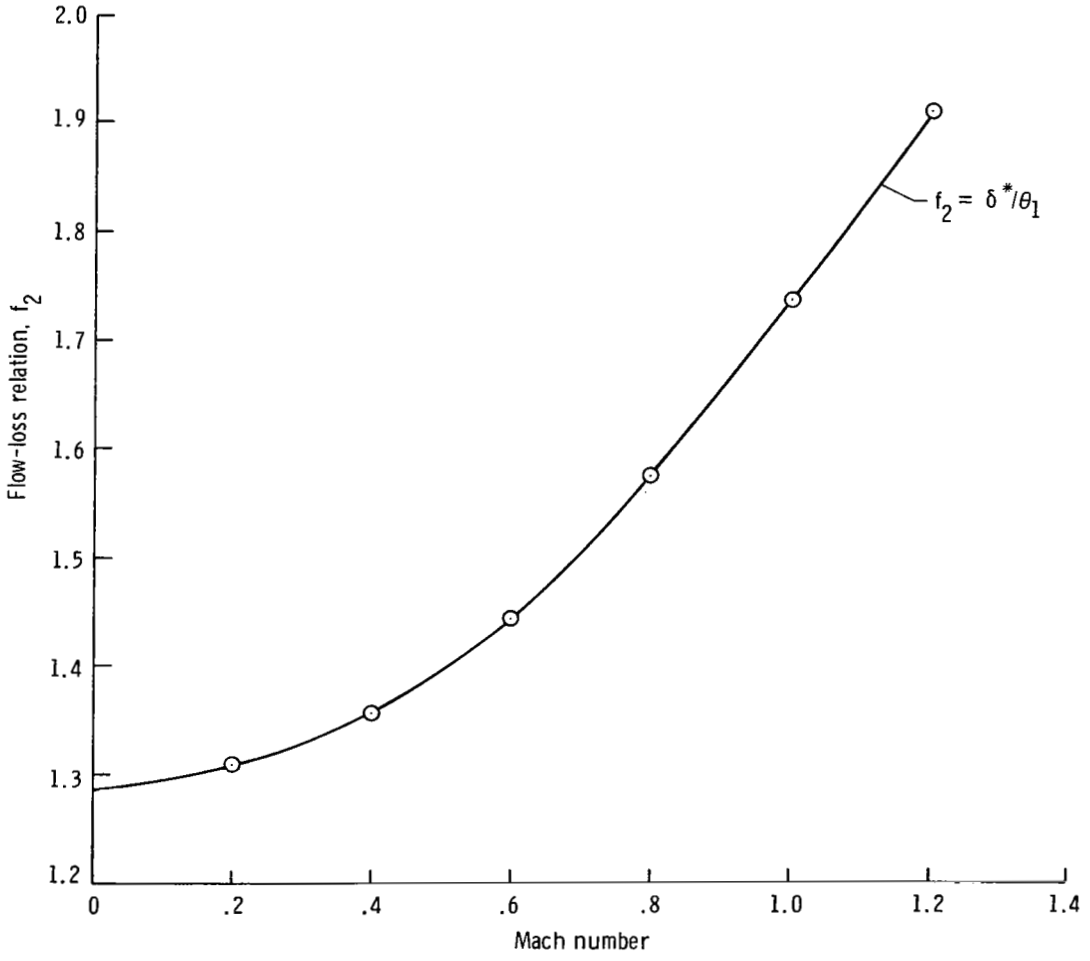

Figure 4.- Variation of f_2 with Mach number.

where L_{TS} is the test-section length and C_D is the drag coefficient for turbulent flow past an insulated flat plate. Shapiro (ref. 12) gives C_D as a function of Mach number and Reynolds number as

$$C_D = 0.472(\log_{10} N_{Re})^{-2.58}(1 + 0.2M^2)^{-0.467} \tag{43}$$

An expression for δ^* as a function of Mach number and Reynolds number can be obtained as

$$\delta^* = \theta_1 f_2(M) = K_\delta f_3(M) \tag{44}$$

where

$$K_\delta = 0.472(\log_{10} N_{Re})^{-2.58} \frac{L_{TS}}{2} \tag{45}$$

and

$$f_3(M) = (1 + 0.2M^2)^{-0.467} f_2(M) \tag{46}$$

Values for $f_2(M)$ and $f_3(M)$ are given in table II and appear as curves in figures 4 and 5. A second-degree polynomial fit to $f_3(M)$, denoted by $f_4(M)$ and tabulated in the rightmost column of table II, is

$$f_4(M) = 1.286 + 0.305M^2 \tag{47}$$

The curves for $f_3(M)$ and $f_4(M)$ coincide in figure 5.

TABLE II.- FLOW-LOSS RELATIONS AS FUNCTIONS OF MACH NUMBER

M	$f_2(M)$	$f_3(M)$	$f_4(M)$
0	1.286	1.286	1.286
.2	1.304	1.299	1.298
.4	1.358	1.338	1.335
.6	1.447	1.401	1.396
.8	1.573	1.487	1.481
1.0	1.734	1.593	1.591
1.2	1.930	1.715	1.725

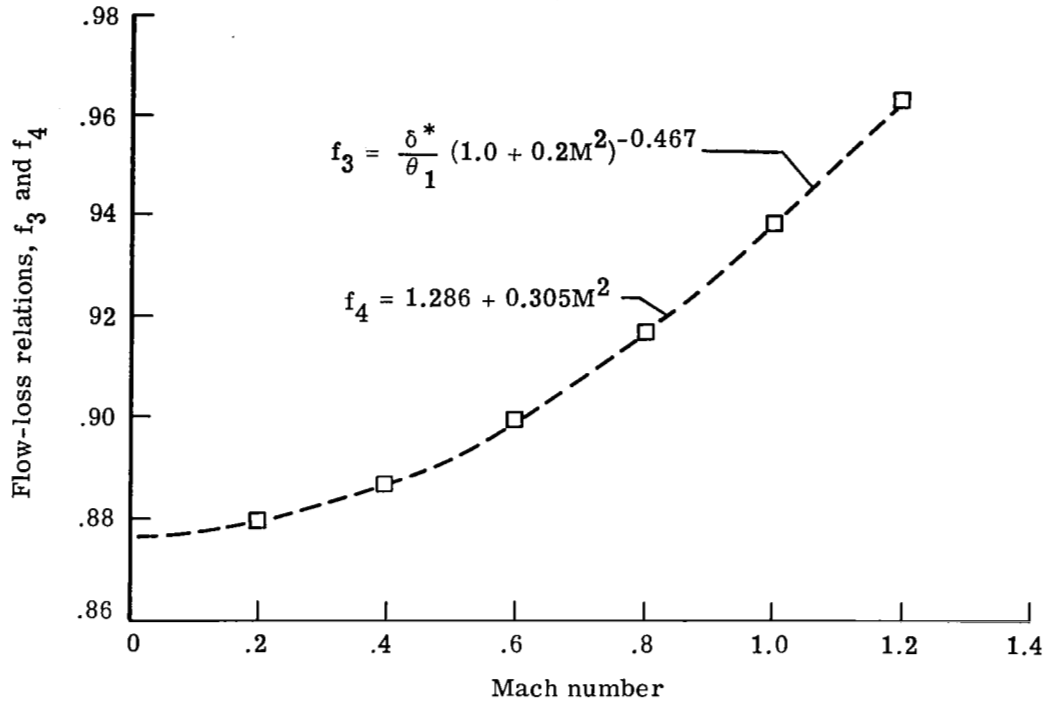

Figure 5.- Variation of f_3 and f_4 with Mach number.

For the second- and third-leg diffusers and the rapid diffuser in the NTF, Rao (ref. 9) obtains a constant diffuser loss factor K of 0.32. In these locations, equation (31) simplifies to

$$\Delta p_t = 0.32 p_1 \left[\left(1 + \frac{\gamma - 1}{2} M^2 \right)^{\frac{\gamma}{\gamma - 1}} - 1 \right] \left(1 - \frac{1}{A_R} \right)^2 \tag{48}$$

The portion of the fan nacelle beyond the fan location is an annular diffuser whose total-pressure loss is computed by Rao for a constant drag coefficient C_D to be

$$\Delta p_t = C_D \left(\frac{1}{2} \rho u^2 \right) \tag{49}$$

where $C_D = 0.158$.

Losses at turning vanes, cooling coils, and screens are also obtained by using equation (49), where values of C_D are given as follows:

Location of loss	C_D
Turning vanes	0.027
Cooling coils	12.0
Screens	3.0

Pressure loss at the strut, also obtained from equation (49), is weighted by the ratio of projected strut frontal area A_S to test-section cross-sectional area A_T, thus giving

$$\Delta p_t = C_D \frac{A_S}{A_T}\left(\frac{1}{2}\rho u^2\right) \tag{50}$$

where $C_D = 0.027$. Pressure losses due to the model and sting are computed similarly as a function of angle of attack.

In each aforementioned case, the total-pressure loss at each diffuser or constricting element is uniformly distributed along its length to obtain a value for $(dp_t/dx)_R$ to be used in equation (28).

SLOTTED-TEST-SECTION DYNAMICS

The flow processes occurring within the slotted test section and plenum of a transonic wind tunnel are not understood well enough to permit construction of an accurate dynamic model. It is clear that the process is asymmetric and three-dimensional with sharp gradients and finely detailed flow patterns. An adequate time-dependent model would require a three-dimensional analysis with a finely spaced grid, which would require lengthy execution on a high-performance digital computer for solution. Such an analysis has not been attempted in the literature as of this writing.

In this study, a one-dimensional approximation to slotted-test-section dynamics is adapted from a lumped model of the NTF slotted-test-section dynamics developed by Gumas. (See ref. 13.) The test section is divided into an exit region (from which slot flow exits into the plenum) which is followed by a reentry region (where flow reenters the test section from the plenum). Slot exit flow is considered by Gumas to consist of three components caused by boundary layer, model blockage, and supersonic effects. Let the lumped exit and reentry mass flows of Gumas be distributed along their corresponding regions. The plenum is considered to be a lumped volume with static plenum pressure uniformly distributed along the exit and reentry regions of the test section, in contrast to the treatment by Gumas of the test-section—plenum combination as a single lumped volume at uniform pressure. This separation of a lumped plenum from a distributed test section introduces another component of slot mass flow proportional to the difference in static pressure between test section and

plenum not included in the formulation of reference 13. The performance of the model for the subsonic case using these assumptions is satisfactory; however, above Mach 1.0 it is less successful, having a tendency toward numerical instability.

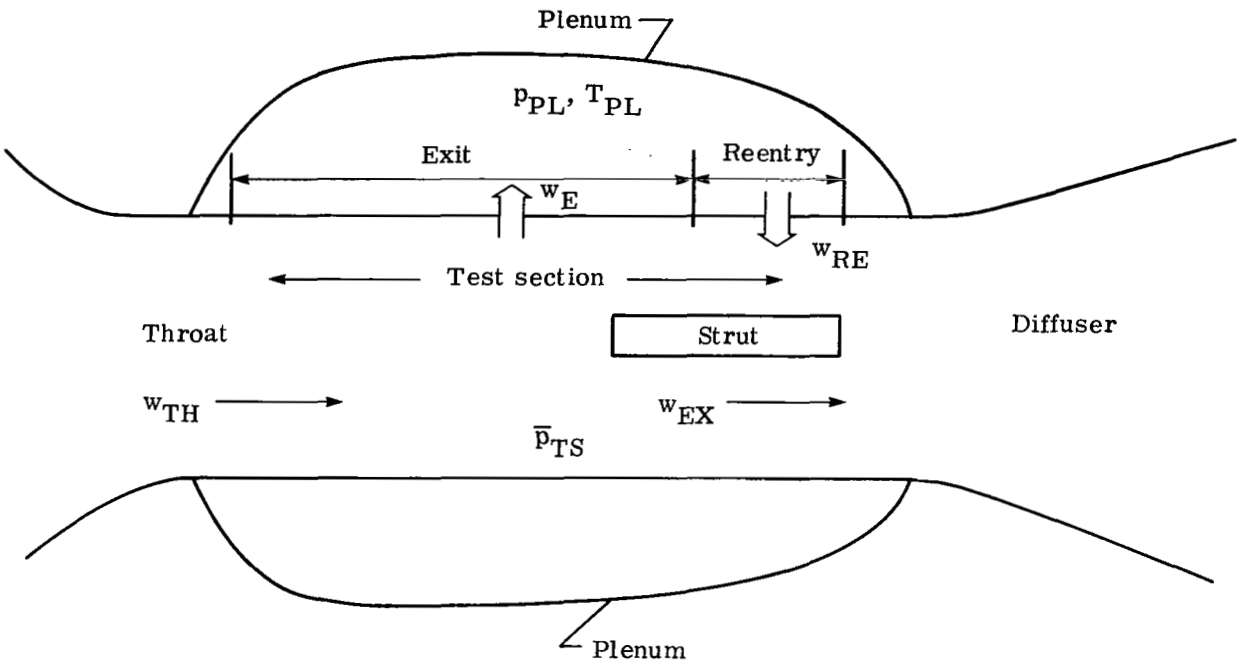

Figure 6.- Slotted test section and plenum.

A diagram of the throat, test section, and plenum regions appears in figure 6. Let w_E denote slot exit (test section to plenum) mass flow which, as mentioned before, according to the Gumas model consists of three components:

(1) The boundary-layer component proportional to throat flow:

$$w_B = C_{XM} w_{TH} \tag{51}$$

(2) The model-blockage component, also proportional to throat flow and dependent on angle of attack:

$$w_{DM} = C_{DMX} w_{TH} \tag{52}$$

(3) The supersonic component, when $M_{TS} > 1.0$:

$$w_{SS} = \left[\left(\frac{5}{6}\right)^3 - \frac{M_{TS}}{\left(1 + 0.2M_{TS}^2\right)^3}\right] p_t A_T \sqrt{\frac{\gamma}{RT_t}} \tag{53}$$

where

w_{TH} average test-section mass-flow rate in throat region

M_{TS} average test-section Mach number in throat region

p_t total pressure

T_t total temperature

A_T test-section cross-sectional area at throat

C_{XM} boundary-layer flow coefficient

C_{DMX} variable model-blockage flow coefficient

The additional pressure-difference flow component w_{ORF} is computed as

$$w_{ORF} = C_{ORF}(\bar{p}_{TS} - p_{PL}) \tag{54}$$

where

$\bar{p}_{TS}$ average static pressure over exit-reentry portion of test section

p_{PL} plenum static pressure

C_{ORF} slot (plenum test-section) pressure-difference flow coefficient

Total slot-exit flow w_E is then

$$w_E = w_B + w_{DM} + w_{SS} + w_{ORF} \tag{55}$$

Note that if the plenum pressure is sufficiently greater than the test-section static pressure, w_E will be negative. Slot exit momentum flow j_E and heat-energy flow q_E are obtained from w_E as

$$j_E = \begin{cases} w_E u_{TS} & (w_E > 0) \\ 0 & (w_E < 0) \end{cases} \tag{56}$$

where u_{TS} is the average test-section stream velocity in the exit region and

$$q_E = \begin{cases} w_E h_{TS} & (w_E > 0) \\ w_E h_{PL} & (w_E < 0) \end{cases} \tag{57}$$

where

$$h_{TS} = c_p T_{TS} \tag{58}$$

$$h_{PL} = c_p T_{PL} \tag{59}$$

and T_{PL} is the plenum temperature.

Reentry mass flow w_{RE} is computed from two components: (1) An extracted component proportional to test-section exit flow

$$w_f = -C_f w_{EX} \tag{60}$$

where w_{EX} is the average test-section mass flow in the reentry region; and (2) the pressure-difference flow component w_{ORF}. Hence, total reentry flow w_{RE} is

$$w_{RE} = w_f - w_{ORF} \tag{61}$$

Reentry momentum flow and energy flow are treated analogously in regard to slot-exit flow. The dynamic state equations for plenum mass and internal energy, respectively, are

$$\dot{m}_{PL} = w_E + w_{RE} \tag{62}$$

and

$$\dot{E}_{PL} = q_E + q_{RE} \tag{63}$$

where

$$q_{RE} = \begin{cases} w_{RE} h_{PL} & (w_{RE} < 0) \\ w_{RE} h_{TS} & (w_{RE} > 0) \end{cases} \tag{64}$$

Plenum temperature T_{PL} is given by

$$T_{PL} = E_{PL}/c_v m_{PL} \tag{65}$$

BOUNDARY CONDITIONS

GN_2 Venting and LN_2 Injection

Next, consider the external mass, momentum, and energy transfer caused by gas venting and liquid-nitrogen injection. Let the vented-gas mass-flow rate be denoted by w_G, and let the influent mass-flow rate per unit length be m'_G. Assume uniform venting over length L_G so that m'_G is given by

$$m'_G = -w_G/L_G \tag{66}$$

The influent momentum-flow rate per unit length j'_G is then

$$j'_G = m'_G u = -w_G u/L_G \tag{67}$$

where u is the local stream velocity at the vent.

Finally, the influent heat-flow rate per unit length q'_G is

$$q'_G = m'_G h_G = -w_G h_G/L_G \tag{68}$$

where h_G, the local total enthalpy, is given by

$$h_G = c_p T + \frac{1}{2} u^2 \tag{69}$$

Corresponding equations for liquid-nitrogen injection can be obtained. Let w_N denote LN_2-injection flow rate (in kilograms per second) occurring uniformly over length L_N. Influent mass-flow rate per unit length denoted by m'_N is then

$$m'_N = w_N/L_N \tag{70}$$

Because the injected liquid nitrogen is assumed to have zero stream velocity at the point of injection, influent momentum-flow rate per unit length j'_N is

$$j'_N = 0 \tag{71}$$

Finally, influent energy per unit length is given by

$$q'_N = m'_N h_N = \frac{w_N h_N}{L_N} \tag{72}$$

where h_N is the total enthalpy of liquid nitrogen. The value used for h_N is -115.9 kJ/kg. Instantaneous vaporization and perfect mixing are assumed.

NTF-Fan Simulation

A one-dimensional approximation to the NTF fan-flow process has been adapted by Gumas (ref. 13) from a three-dimensional fan model. In the approximation by Gumas, fan volumes are assumed to be insignificant relative to the tunnel volume; mass, momentum, and energy relations between fan-inlet flow and fan-outlet flow are assumed to be algebraic functions dependent on fan speed ν and inlet-guide-vane position α. Thus, the fan model has no intrinsic dynamics. Inlet-guide-vane actuator dynamics are modeled as a second-order linear dynamical system. Fan-drive dynamics are not included in the present model because constant fan speed is assumed.

The functional relations between fan-inlet and fan-outlet flows established by the Gumas fan model establish the relation between the outlet and inlet flows of the closed-return wind tunnel. This can be represented formally as a vector-function equation. In this solution, let V denote the vector of three independent flow properties

$$V = \begin{bmatrix} \rho\omega \\ \rho u\omega \\ e_t\rho\omega \end{bmatrix} \tag{73}$$

where subscripts 1 and N denote tunnel inlet and tunnel outlet, respectively. Also, let G be the vector function representing fan-outlet flow as a function of fan-inlet flow, fan speed, and inlet-guide-vane position. Then, the relation between V_1 (the vector of tunnel-inlet flow properties) and V_N (the vector of tunnel-outlet flow properties) is expressed by

$$V_1 = G(V_N, \alpha, \nu) \tag{74}$$

The relationships symbolized by vector function G and its inverse G^{-1} determine the boundary conditions at the ends of the one-dimensional tube. Functions G and G^{-1} are evaluated numerically by means of a computer subroutine.

NUMERICAL SOLUTION OF FLOW EQUATIONS

Equations (8), (16), and (18) are solved numerically to obtain a time-dependent solution of the wind-tunnel flow process. For notational convenience, these equations are written in conservation form as

$$\frac{\partial}{\partial t} V(x,t) + \frac{\partial}{\partial x} F(x,t) + H(x,t) = 0 \tag{75}$$

where

$$F = \begin{bmatrix} \rho u\omega \\ \rho u^2\omega + p\omega - \frac{4}{3}\mu\omega\frac{\partial u}{\partial x} \\ e_t\rho u\omega + pu\omega - k\omega\frac{\partial T}{\partial x} - \frac{4}{3}\mu u\omega\frac{\partial u}{\partial x} \end{bmatrix} \tag{76}$$

and

$$H = \begin{bmatrix} -m' \\ -p\frac{d\omega}{dx} - j' \\ -q' \end{bmatrix} \tag{77}$$

A second-order explicit predictor-corrector method developed by MacCormack (ref. 14) is employed to obtain a numerical solution to equation (75). In this method, let the length of the tube be divided into N equal segments of length Δx and let Δt_i denote the time increment at the time step i. Let the diacritical marks $\sim$ and $\wedge$ denote predicted and corrected values, respectively, of the variables. Let subscript n denote the values of the variables at station x_n where

$$x_n = n\,\Delta x \qquad (n = 0, \ldots, N) \tag{78}$$

and let superscript k denote the values of variables at time t_k where

$$t_k = \sum_{i=1}^{k} \Delta t_i \qquad (k = 0, 1, 2, \ldots) \tag{79}$$

so that the predicted value is

$$\tilde{V}_n^k = \tilde{V}(x_n, t_k) \tag{80}$$

and the corrected value is

$$\hat{V}_n^k = \hat{V}(x_n, t_k) \tag{81}$$

MacCormack's method (ref. 14) proceeds as follows for $n = 2, 3, \ldots, N-1$:

(1) Predictor step:

$$\tilde{V}_n^{k+1} = V_n^k - \left[\left(F_n^k - F_{n-1}^k\right)\frac{1}{\Delta x} + H_n^k\right]\Delta t \tag{82}$$

(2) Corrector step:

$$\hat{V}_n^{k+1} = V_n^k - \left[\left(\tilde{F}_{n+1}^{k+1} - \tilde{F}_n^{k+1}\right)\frac{1}{\Delta x} + \tilde{H}_n^{k+1}\right]\Delta t \tag{83}$$

(3) Update step:

$$V_n^{k+1} = \frac{1}{2}\left(\tilde{V}_n^{k+1} + \hat{V}_n^{k+1}\right) \tag{84}$$

Because partial derivatives occur in vector function F, additional differencing is necessary within F_n^k and $\tilde{F}_n^k$. In MacCormack's formulation, these derivatives are written, respectively, as

$$F_n^k = \begin{bmatrix} \rho_n u_n \omega_n \\ \left[\rho_n u_n^2 + p_n - \frac{4}{3}\mu(u_{n+1} - u_n)\frac{1}{\Delta x}\right]\omega_n \\ \left[e_{t,n}\rho_n u_n + p_n u_n - k(T_{n+1} - T_n)\frac{1}{\Delta x} - \frac{4}{3}\mu(u_{n+1} - u_n)\frac{1}{\Delta x}\right]\omega_n \end{bmatrix} \tag{85a}$$

and

$$\tilde{F}_n^k = \begin{bmatrix} \tilde{\rho}_n \tilde{u}_n \omega_n \\ \left[\tilde{\rho}_n \tilde{u}_n^2 + \tilde{\rho}_n - \frac{4}{3}\mu(\tilde{u}_n - \tilde{u}_{n-1})\frac{1}{\Delta x}\right]\omega_n \\ \left[\tilde{e}_{t,n}\tilde{\rho}_n \tilde{u}_n + \tilde{\rho}_n \tilde{u}_n - k(\tilde{T}_n - \tilde{T}_{n-1})\frac{1}{\Delta x} - \frac{4}{3}\mu(\tilde{u}_n - \tilde{u}_{n-1})\frac{1}{\Delta x}\right]\omega_n \end{bmatrix} \tag{85b}$$

The wind tunnel is a closed-return tube driven by a fan. As discussed previously, the fan is represented by a vector-function relation G between vectors V_N and V_1 so that

$$V_1 = G(V_N) \tag{86}$$

From stations x_N to x_1, the predictor-corrector steps are the following:

(1) Predictor step:

$$\tilde{V}_N^{k+1} = V_N^k - \left[\left(F_N^k - F_{N-1}^k\right)\frac{1}{\Delta x} + H_N^k\right]\Delta t \tag{87}$$

$$\tilde{V}_1^{k+1} = G\left(\tilde{V}_N^{k+1}\right) \tag{88}$$

(2) Corrector step:

$$\hat{V}_1^{k+1} = V_1^k - \left[\left(\tilde{F}_2^{k+1} - \tilde{F}_1^{k+1}\right)\frac{1}{\Delta x} + \tilde{H}_1^{k+1}\right]\Delta t \tag{89}$$

(3) Update step:

$$V_1^{k+1} = \frac{1}{2}\left(\tilde{V}_1^{k+1} + \hat{V}_1^{k+1}\right) \tag{90}$$

$$V_N^{k+1} = G^{-1}\left(V_1^{k+1}\right) \tag{91}$$

where G^{-1} denotes the inverse of vector function G.

The time increment Δt is recomputed after each time step with the relation

$$\Delta t = \frac{0.9\ \Delta x}{\max\ (|u| + a)} \tag{92}$$

where a is the local speed of sound and max denotes maximum value.

Above a Mach number of 1.0, shocks form in the test section and produce rapid numerical changes which can lead to computational instability. Artificial viscosity is introduced into the computation to smooth the shock discontinuity to a continuous change over several spatial increments. In the present treatment, an artificial-viscosity computation method furnished by Turkel (ref. 15) is used. In this method, the following functions of time step k and spatial index n are defined as

$$C_T^k = \frac{C_X\ \Delta t^k}{\Delta x} \tag{93}$$

$$d_{u,n}^k = \left|u_{n+1}^k - u_n^k\right| \tag{94}$$

$$D_{V,n}^k = V_{n+1}^k - V_n^k \tag{95}$$

$$P_{V,n}^k = C_T^k d_{u,n}^k D_{V,n}^k \tag{96}$$

The artificial-viscosity vector U_n^{k+1}, given by

$$U_n^{k+1} = P_{V,n}^k - P_{V,n-1}^k \tag{97}$$

is added to the updated state vector V_n^{k+1}, given in equation (84), to yield the smoothed state vector

$$\left(V_n^{k+1}\right)_s = V_n^{k+1} + U_n^{k+1} \qquad (n = 2, \ldots, N-1) \tag{98}$$

No smoothing is done at stations x_1 and x_N.

The aforementioned numerical application of MacCormack's predictor-corrector method has been implemented on a CDC CYBER 203 digital computer. (See ref. 4 by Lambiotte and Howser.) Vector equations (82) and (84) are well-suited for vectorization on this computer because each vector-addition and vector-multiplication operation is performed by a single machine instruction for vectors of lengths up to 64 000 elements. For the NTF model, the x-coordinate is divided into 512 segments. Because each of the three elements of vector V_n^k for $n = 2$ through 511 in equations (82) through (84) undergoes the same arithmetic operation, a single machine instruction is sufficient to perform the arithmetic operation on the entire set of 1530 elements referenced in vectors V_2 through V_{511}. Separate operations are needed at stations 1 and 512 as given in equations (86) through (91). However, the elimination of 1530 separate addition or multiplication instructions for each vector addition or multiplication operation in equations (82) through (84), along with loop-control instructions, results in a significant reduction in computing time.

The proportion of scalar to vector operations in a program determines the extent of speedup over a serial program. Because the solution of the basic equations of flow is highly vectorized, a speedup factor of 50 to 60 is realized for the portion of the program corresponding to equations (82) through (84). However, because simulation of the actuator and feedback-control dynamics used in the present study is not vectorizable, inclusion of those features results in a larger proportion of nonvector operations. The complete simulation, including actuators and controls, requires an average 0.006 sec of machine execution time per simulated time step Δt. The value of Δx is 0.295 m. From equation (92), it follows that

$$\Delta t = \frac{0.266}{\max\left(|u| + a\right)} \tag{99}$$

A typical value of Δt at a Mach number of 0.8 and total temperature of 333 K is 0.0004 sec. Thus, simulation of 1 sec of tunnel-control dynamics requires approximately 15 sec on the central processing unit (CPU). At lower Mach numbers and temperatures, Δt becomes larger. For example, at a Mach number of 0.8 and temperature of 167 K, Δt is 0.0005, and 12 CPU sec are required for each simulated tunnel second. In simulations of the Langley 0.3-Meter Transonic Cryogenic Tunnel, 256 segments were used, which reduced execution times by a factor of 4 over that required for simulation of the NTF wind tunnel.

INITIAL CONDITIONS

Initial steady-flow conditions are obtained by integration of the steady-flow equations (A1) through (A3) of the appendix with an Adams method. (See ref. 16 by

Hindmarsh.) Generally, some combination of steady-flow initial values of Mach number, total temperature, and total pressure at the test section are desired. However, values of state variables can be specified only at the tunnel inlet, along with GN_2-vent flow rate w_G and LN_2-injection flow rate w_N. At steady flow it is seen that w_G must equal w_N. Furthermore, the values of w_G and w_N must be such that fan work added to the enthalpies removed by LN_2 injection and GN_2 venting equals zero. Thus, values of tunnel-inlet state variables must be selected which will produce a tunnel energy balance and the required values of M, T_t, and p_t in the test section.

It is convenient to employ T_t as an indicator of energy balance at the fan. It can be shown that for steady flow, T_t remains constant along the tunnel circuit except at the LN_2 spray bar and across the fan. Fan-outlet total temperature is given by

$$T_{t,F} = \frac{\left(r_F^{\frac{\gamma-1}{\gamma}} - 1\right)T_{t,N}}{\eta_F} + T_{t,N} \tag{100}$$

where

r_F fan compression ratio

η_F fan efficiency

$T_{t,N}$ fan-inlet total temperature

Because η_F is known and r_F is computed from the ratio of total pressures

$$r_F = p_{t,1}/p_{t,N} \tag{101}$$

where $p_{t,N}$ denotes tunnel-outlet total pressure and $p_{t,1}$ denotes tunnel-inlet total pressure, $T_{t,F}$ can be computed from the integrated solution of equations (A1) through (A3). Thus, a procedure for obtaining initial conditions is as follows: (1) Select values of ρ_1, u_1, $e_{t,1}$, and w_G; (2) integrate equations (A1) through (A3); and (3) compute M_{TS}, $p_{t,TS}$, $T_{t,TS}$, and $T_{t,F}$. Since, at steady flow, $T_{t,F}$ must equal $T_{t,1}$, by means of some type of organized search procedure, such as a gradient method, update ρ_1, u_1, $e_{t,1}$, and w_G and iterate until $T_{t,F}$ equals $T_{t,1}$ and M_{TS}, $p_{t,TS}$, and $T_{t,TS}$ equal the required values.

SIMULATION STUDIES

The Langley 0.3-Meter Transonic Cryogenic Tunnel

The Langley 0.3-Meter Transonic Cryogenic Tunnel (0.3-m TCT) has previously been simulated by means of a hybrid dynamic model by Thibodeaux and Balakrishna. (See ref. 17.) Although the scales and dynamic time constants of the NTF and 0.3-m TCT facilities differ by an order of magnitude, Mach number, temperature, and pressure ranges are comparable. Table III lists parameters for the 0.3-m TCT and the NTF.

TABLE III.- PARAMETERS FOR THE 0.3-m TCT AND THE NTF WIND TUNNEL

Parameter	Wind tunnel	
	0.3-m TCT	NTF
Test-section area, m^2	0.124	6.25
Tunnel circuit length, m ...	21.7	151.2
Tunnel volume, m^3	14	5597
Plenum volume, m^3	0.680	907
Mass of liner, kg	3200	465 000
Temperature range, K	80 to 325	78 to 340
Pressure range, atm	1.1 to 6.0	1.0 to 9.0
Mach number range	0.2 to 0.98	0.2 to 1.2
Maximum Reynolds number per 0.25 m	90×10^6	120×10^6
Circuit time, sec:		
M = 1, T = 300 K	0.6	4.8
M = 0.2, T = 100 K	3.0	24

Furthermore, the basic circuit geometries are similar, boundary interfaces are of the same type, and the fans, GN_2 vents, and LN_2 spray bars are in the same relative positions in the 0.3-m TCT (fig. 7) and in the NTF wind tunnel (fig. 1). Because of reduced computer execution times required for the smaller 0.3-m TCT, preliminary simulation studies were performed using 0.3-m parameters and a simplified fan representation in the model. Some typical results of these studies are now described.

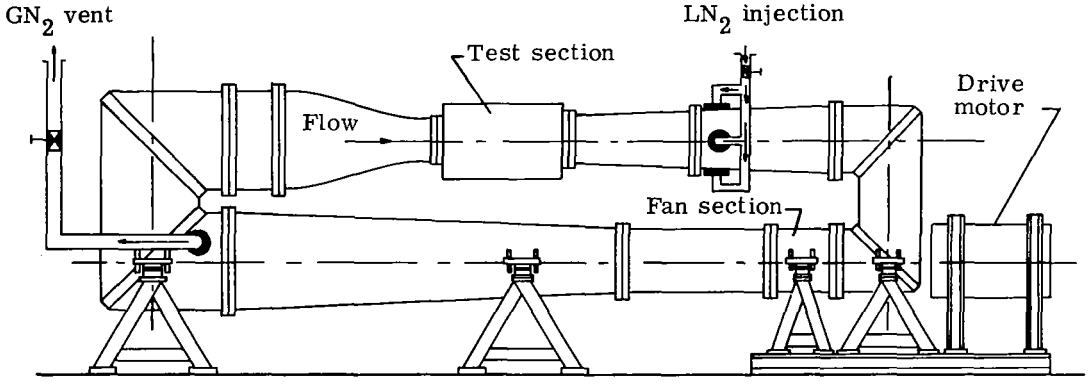

Figure 7.- Schematic diagram of Langley 0.3-Meter Transonic Cryogenic Tunnel.

Pulsed upsets of 3-sec duration in fan compression ratio, GN_2-vent flow rate, and LN_2-injection flow rate from steady-flow conditions have been simulated. Because fan drive and valve actuator dynamics were not included in this 0.3-m simulation, these upsets are represented as idealized rectangular pulses, which result in the flow responses shown in figures 8, 9, and 10. Computed responses to a 3-sec pulsed decrement in fan compression ratio appear in figure 8 at 277 K, 5 atm, and Mach 0.69. The computed responses, which show temporary decreases in total temperature, total

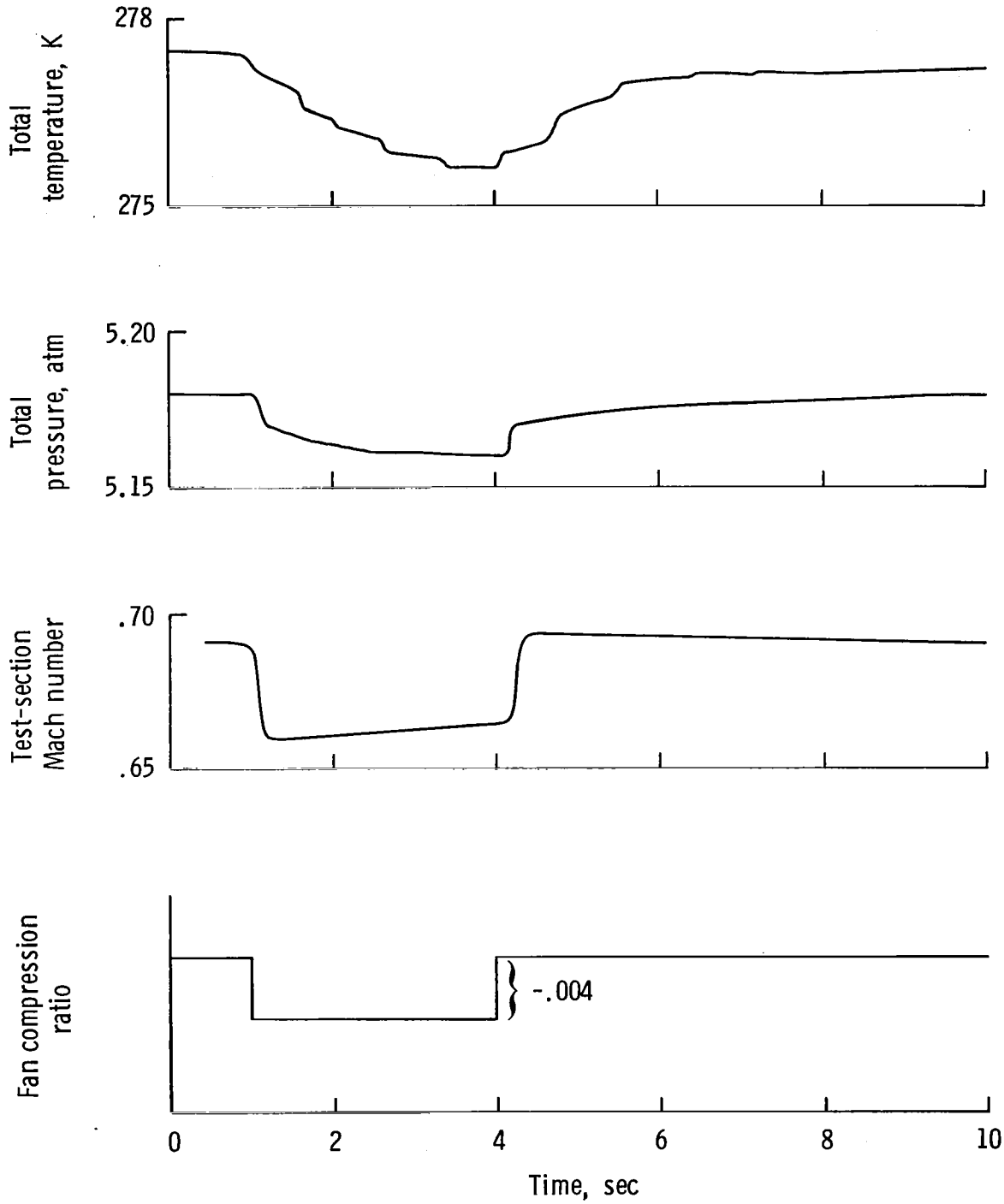

Figure 8.- Computed response of 0.3-m TCT to fan compression-ratio upset.

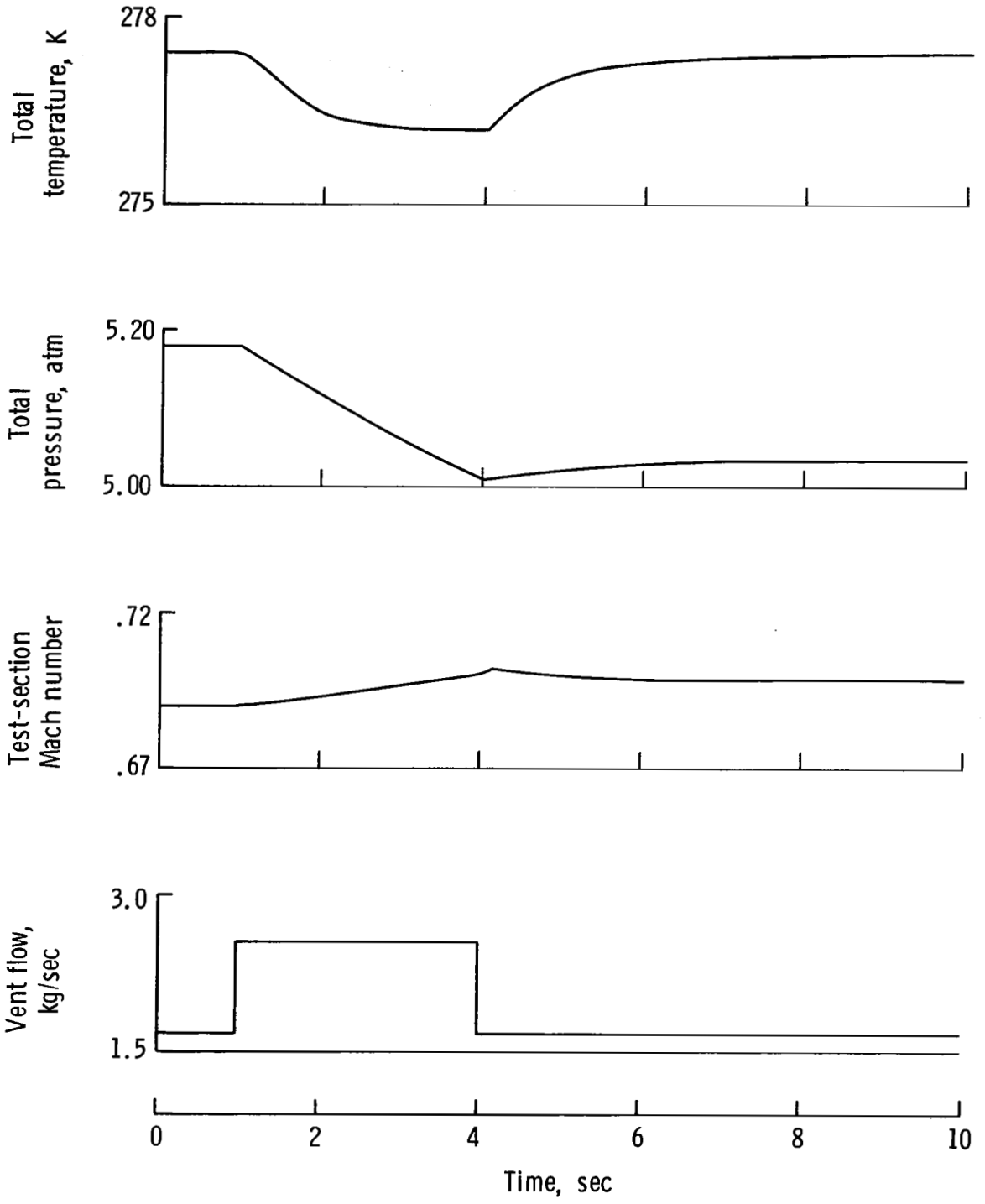

Figure 9.- Computed response of 0.3-m TCT to vent-flow upset.

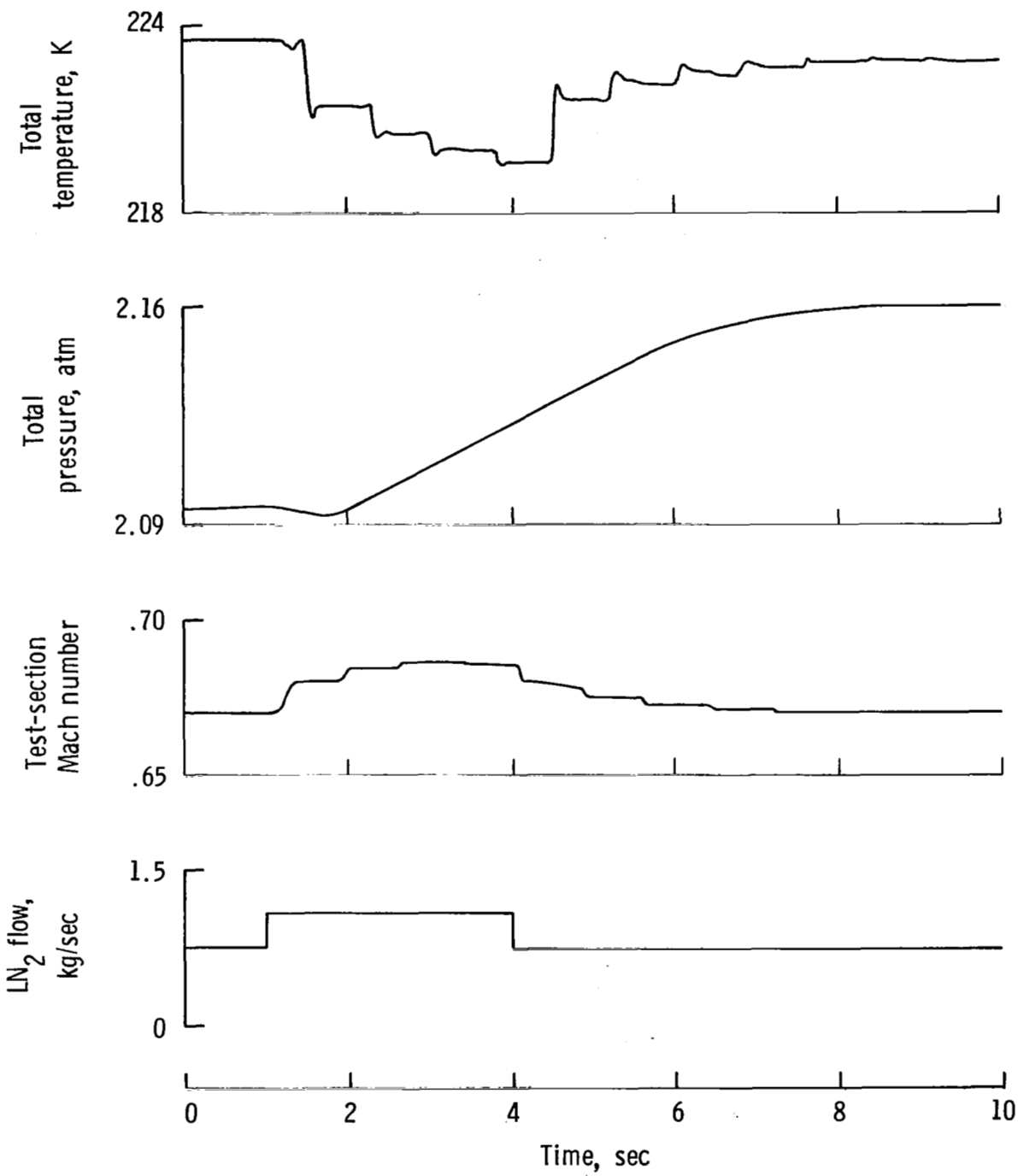

Figure 10.- Computed response of 0.3-m TCT to LN_2-flow upset.

pressure, and Mach number, are very nearly rectangular because of the omission of actuator dynamics. Figure 9 contains the computed responses to a 3-sec pulsed increment in GN_2-vent flow at 277 K, 5 atm, and Mach 0.7.

Figure 10 shows the computed responses to a 3-sec pulsed increment in LN_2 flow at approximately 224 K, 2.1 atm, and Mach 0.67. These responses show an initial rapid decrease in total temperature followed by a slower recovery. Total pressures exhibit a very small initial drop followed by a sizable increase. Mach numbers show a pulsed increment during the LN_2 pulse followed by quick recovery to the original value. The computed temperature response exhibits temperature fronts which propagate at stream velocity as predicted theoretically. Temperature fronts were not observed experimentally in the 0.3-m TCT in tests which employed thermocouple temperature transducers with time constants of approximately 0.5 to 1.0 sec. Additional tests employing faster-response thermocouples are planned as of this writing.

The computed temperature fronts decay after 3 to 4 tunnel circuit times because of heat transfer between the gas and the tunnel liner. Without gas-to-liner heat transfer, the amplitude of the steps would not be attenuated with time.

Temperature fronts have been observed experimentally in the T'2 cryogenic wind tunnel at the Toulouse Research Center, Toulouse, France. (See ref. 2 by Blanchard, Dor, and Breil.) The fronts seen at Toulouse, induced by a step change of -36 percent in LN_2 flow, were observed to propagate at stream velocity. They had decayed after two tunnel circuits, and the leading edges had become longitudinally diffuse near the end of their existence. Analytic solutions of the flow equations predict such temperature fronts, confirming the numerical result. Determination of their existence in the NTF must await experimentation after its completion.

NTF Actuator, Sensor, and Control Studies

The mechanical actuators for GN_2-vent valves, LN_2-inlet valves, and inlet guide vanes in the NTF have been modeled by Gumas (ref. 13) as second-order linear systems. Valve stroke-flow calibrations have been provided as functions of local stagnation, supply, and vent pressures. Also, two types of high-accuracy pressure transducers were dynamically modeled by Gumas: a sonar mercury manometer and a quartz bourdon-tube transducer. Both systems have dynamic-response times of several seconds. Temperature transducers are modeled as first-order linear systems with time constants of 0.63 sec.

Three discrete sampled-data feedback control loops of the proportional-integral (PI) type with variable feedback gains for controlling stagnation pressure, stagnation temperature, and Mach number in the NTF were developed by Gumas. Stagnation pressure is regulated by a GN_2-vent-valve control loop; stagnation temperature, by an LN_2-inlet-valve control loop; and Mach number, by a fan inlet-guide-vane control loop. Nominal sampling-time increments are 0.1 sec for the pressure and Mach number control loops and 0.04 sec for the temperature control loop.

The Gumas simulations of actuators, transducers, and feedback controls have been appended to the distributed-parameter NTF model. In order for the computations to be synchronized, the ordinary differential equations describing actuator dynamics are solved with simple Euler integration for a time step Δt_i equal to that of the MacCormack method (ref. 14) for solving the partial differential equations. The small value of Δt_i ensures adequate accuracy.

A large number of experimental simulation studies have been performed to evaluate the performance of the Gumas control laws at selected values of Mach number, temperature, and pressure. Typical runs simulate programmed set-point changes under automatic control in Mach number, total temperature, and total pressure with the other two variables fixed. Performance criteria, which require minimum settling time for the controlled variable and minimum upset in the fixed variables, may thus be tested. Figures 11 through 14 show simulated results for selected test cases. Figure 11 shows a controlled Mach number change from 0.8 to 0.9 at 2.04 atm and 333.3 K. The Mach number set-point command occurs at 5 sec; the settling time to a Mach number of 0.900 is approximately 15 sec. Upsets in p_t at T_t are minimal, less than 0.0013 atm and 0.167 K, respectively. Computed time histories of sensed test-section Mach number, total temperature, total pressure, inlet-guide-vane position, LN_2-valve position, and GN_2-valve position are shown.

Figures 12 and 13 illustrate a controlled temperature transition from 166.7 K to 178.9 K for a Mach number of 0.8 at 2.04 atm. The temperature set-point command occurs at 5 sec, and the transition time is approximately 37 sec. Figure 12 contains actuator positions for guide-vane angle, LN_2, and GN_2, along with test-section Mach number, total pressure, and total temperature, the latter exhibiting well-defined temperature fronts. Pressure variation during the temperature transition is less than 0.0013 atm; Mach number variation is less than 0.004. Figure 13 shows the propagation of the temperature fronts, moving at stream velocity, at five stations along the NTF circuit. The fronts decay within six tunnel circuit times.

Figure 14 shows a controlled pressure transition from 2.04 to 1.85 atm for a Mach number of 0.6 at 166.7 K. The pressure set-point command occurs at 5 sec. The pressure transition time is approximately 7 sec; however, Mach number and temperature disturbances require 11- and 13-sec settling times, respectively. It is seen that a significant temperature pulse of -3.3-K amplitude and 13-sec duration is introduced by the controlled pressure transition. Likewise, a Mach number upset of 0.010 amplitude occurs. Thus, although the Mach number and temperature control loops, which regulate inlet-guide-vane positions and LN_2-inlet-valve position, do not appreciably interact with the GN_2 control loop, the latter control loop interacts significantly with the other two loops in regulating the vent-valve position.

The simulated effects of a hypothetical guide-vane upset on steady controlled flow in the NTF are seen in figure 15. A 2.5° step pulse in inlet-guide-vane position of 2-sec duration is applied with Mach number controls fixed but temperature and pressure controls active. A significant Mach number transient results which decays after 10 sec. However, a train of temperature-impulsive disturbances of 2-K to 3-K amplitude is established which does not decay with time. It can be seen from the valve-position records that the reaction of the controls to the temperature impulses tends to reinforce and maintain their existence. This test case demonstrates the need for the carefully programmed Mach number transition control which was designed into the actual NTF control system.

The effect of control-loop sampling rate on control performance was investigated in a series of simulations. The nominal values of the sampling intervals quoted previously were determined to be the largest values allowable for acceptable performance. Longer sampling intervals were found to cause slower control response, increased overshoot, and excessive oscillation. Sampling intervals of 0.5 sec or greater caused the control loops to become unstable.

In a study by Armstrong and Tripp (ref. 18), multivariable-design techniques are applied to Mach number control of the NTF wind tunnel. In particular, optimal

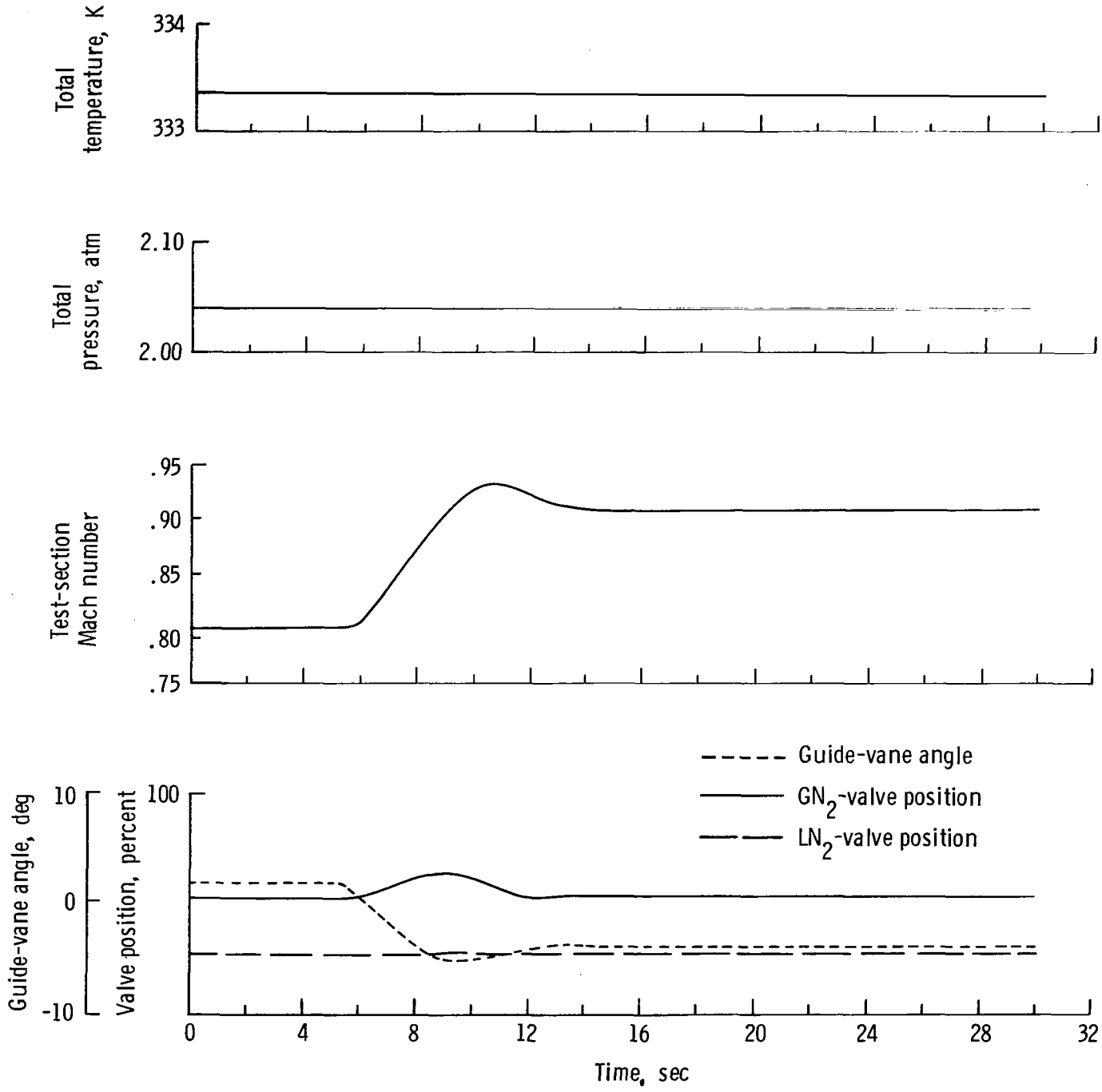

Figure 11.- Simulation of controlled Mach number as predicted by NTF model.

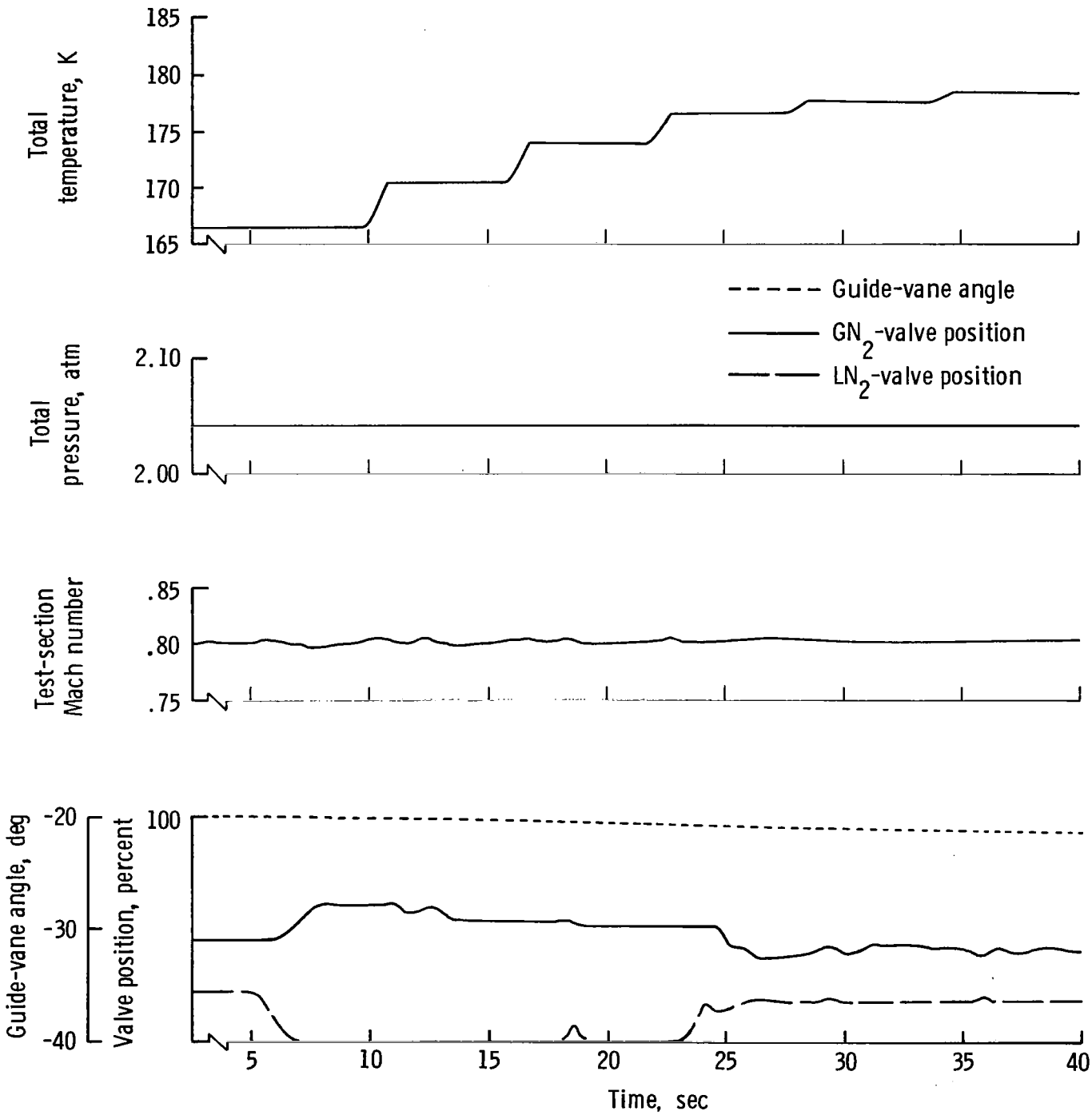

Figure 12.- Simulation of controlled temperature transition as predicted by NTF model.

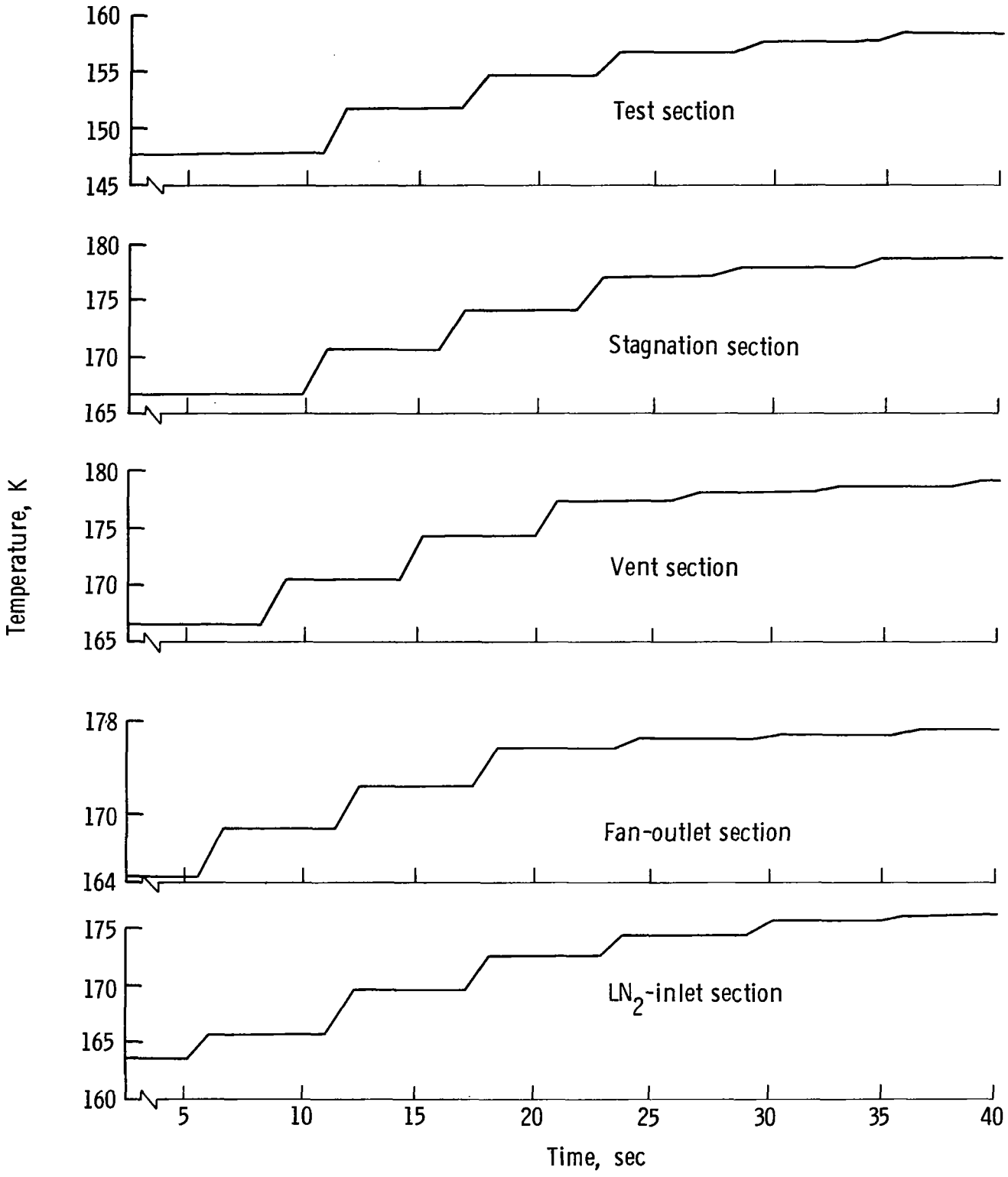

Figure 13.- Propagation of temperature fronts in NTF circuit as predicted by present model.

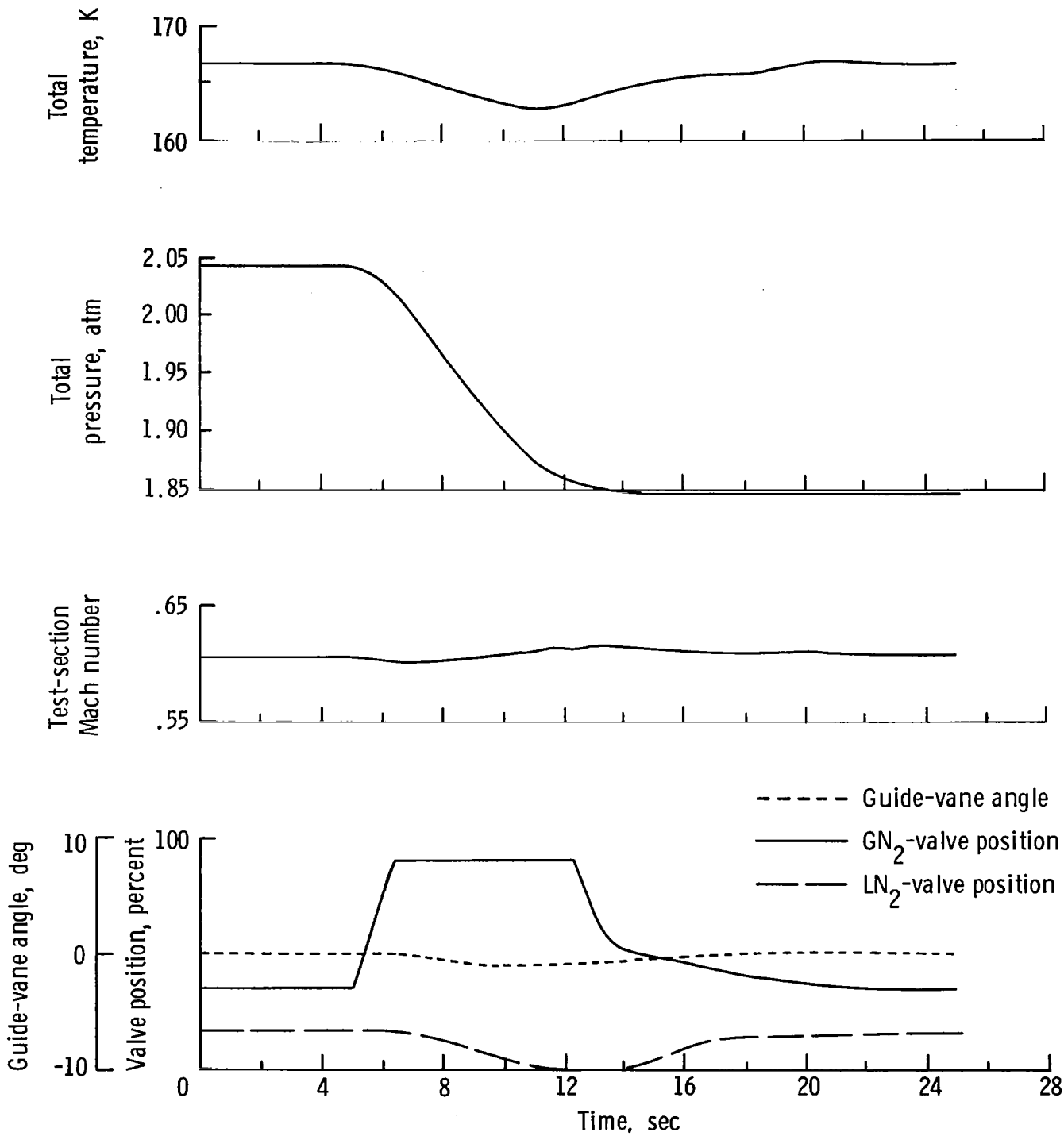

Figure 14.- Simulation of controlled pressure transition as predicted by NTF model.

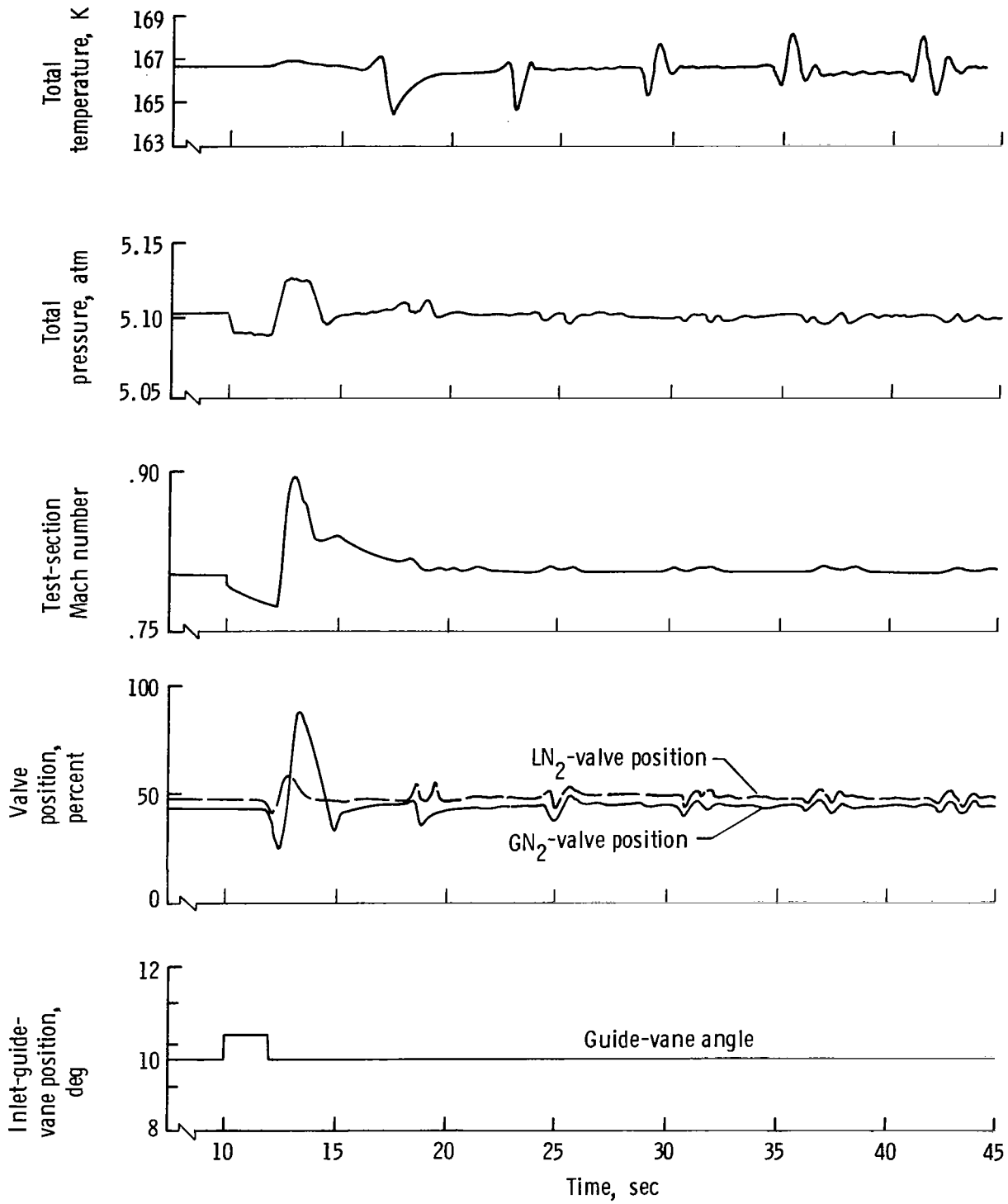

Figure 15.- Simulated Mach number upset with guide-vane controls fixed as predicted by NTF model.

linear-regulator theory and eigenvalue-placement theory are employed to develop Mach number control laws, which are evaluated by using the distributed-parameter simulation described herein with actuator dynamics included. The resulting Mach number control law is found to reduce settling time significantly over that achieved by a conventional proportional-integral control loop. Details of the performance comparisons described here appear in reference 18.

CONCLUDING REMARKS

The three-dimensional equations of fluid flow in integral form have been applied to a differential element of a one-dimensional tube of varying cross-sectional area. Heat-transfer effects due to thermal conductivity and viscous terms have been introduced to derive a one-dimensional system of partial differential equations analogous to the three-dimensional Navier-Stokes equations, which were applied to wind-tunnel geometry. The increase in entropy along the length of the tube was seen to be caused by a viscous momentum loss. This momentum loss, manifested as a loss in total pressure, was quantified from empirical pressure-loss relations obtained for diffusers, turning vanes, screens, and cooling coils in the National Transonic Facility (NTF) wind tunnel at the Langley Research Center. The cryogenic wind tunnels to be modeled contain a slotted test section whose analysis is based on a lumped model wherein the plenum is represented as a lumped volume. The model is extended by separating the lumped plenum from the distributed test section and by distributing slot flow and the test-section length.

The NTF and the Langley 0.3-Meter Transonic Cryogenic Tunnel are simulated by means of this model. A one-dimensional model of the fan adapted from a three-dimensional fan model is employed to relate the inlet-outlet values of mass, momentum, and energy flow rates in the one-dimensional tube. Fan compression ratio, determined by fan speed and an inlet-guide-vane system, establishes Mach number. Temperature control is effected by means of a liquid-nitrogen inlet spray bar and control valve. Pressure is maintained by a vent control valve. Inlet-guide-vane and control-valve actuators are modeled as second-order linear systems.

The partial differential equations of the distributed parameter model are solved numerically by using an explicit, second-order, finite-difference, predictor-corrector method. The lumped ordinary differential equations describing actuator and control dynamics are solved by simple Euler integration synchronized with the finite-difference computation.

The model has been employed in the development of multivariable control techniques based on optimal-regulator theory and eigenvalue-placement theory. (See NASA TP-1887.) It has been employed extensively in the development of digital-process control algorithms for controlling Mach number, total pressure, and total temperature in the NTF wind tunnel.

Langley Research Center
National Aeronautics and Space Administration
Hampton, VA 23665
July 6, 1983

APPENDIX

SOME STEADY-FLOW RELATIONSHIPS

The differential equations for one-dimensional steady flow are

$$\frac{d}{dx}(\rho u \omega) = m' \tag{A1}$$

$$\frac{d}{dx}(\rho u^2 \omega + p\omega) = p \frac{d\omega}{dx} + j' \tag{A2}$$

$$\frac{d}{dx}(e_t \rho u \omega + pu\omega) = q' \tag{A3}$$

Equations (A1) and (A2) can be written, respectively, as

$$\frac{du}{dx} + \frac{u}{\rho}\frac{d\rho}{dx} = -\frac{u}{\omega}\frac{d\omega}{dx} + \frac{m'}{\rho\omega} \tag{A4}$$

and

$$u\frac{du}{dx} + \frac{1}{\rho}\frac{d\rho}{dx} = \frac{j' - um'}{\rho\omega} \tag{A5}$$

Total enthalpy h_t is defined as

$$h_t = e + \frac{p}{\rho} + \frac{1}{2}u^2 \tag{A6}$$

where e is the internal energy per unit mass. Equation (A3) becomes

$$\frac{d}{dx}(h_t \rho u \omega) = q' \tag{A7}$$

or

$$u\frac{dh_t}{dx} = \frac{q' - h_t m'}{\rho\omega} \tag{A8}$$

For an ideal gas, the total enthalpy can be written as

$$h_t = \frac{\gamma}{\gamma - 1}\frac{p}{\rho} + \frac{1}{2}u^2 \tag{A9}$$

APPENDIX

With substitution of equation (A9), equation (A8) can be written as

$$\frac{u}{\rho}\frac{d\rho}{dx} = \frac{u}{\rho}\frac{dp}{dx} + \frac{\gamma - 1}{\gamma}\frac{\rho u^2}{p}\frac{du}{dx} - \frac{\gamma - 1}{\gamma}\left(\frac{q' - h_t m'}{p\omega}\right) \tag{A10}$$

This expression can be substituted into equation (A4) to yield

$$\frac{du}{dx} + \frac{u}{\gamma p}\frac{dp}{dx} = -\frac{u}{\omega}\frac{d\omega}{dx} + \frac{\gamma - 1}{\gamma p\omega}\left(q' + \frac{1}{2}u^2 m' - uj'\right) \tag{A11}$$

Equations (A5) and (A11) are solved simultaneously to eliminate du/dx so that

$$\left(1 - \frac{1}{\gamma}\frac{\rho u^2}{p}\right)\frac{dp}{dx} = \frac{\rho u^2}{\omega}\frac{d\omega}{dx} + \frac{1}{\omega}(j' - um') - \frac{\gamma - 1}{\gamma}\frac{\rho u}{p\omega}\left(q' + \frac{1}{2}u^2 m' - uj'\right) \tag{A12}$$

It is desired to obtain a steady-flow expression for the gradient of total pressure dp_t/dx in terms of m', j', and q'. Equation (A12) will be found to be useful to that end. The defining equation for p_t is

$$p_t = p\left(1 + b\frac{\rho u^2}{p}\right)^{\frac{\gamma}{\gamma - 1}} \tag{A13}$$

where

$$b = \frac{\gamma - 1}{2\gamma} \tag{A14}$$

Differentiation of equations (A2) and (A13) and considerable manipulation yield

$$\frac{dp_t}{dx} = \frac{1}{2}\left(1 + b\frac{\rho u^2}{p}\right)^{\frac{1}{\gamma - 1}}\left[\left(1 - \frac{1}{\gamma}\frac{\rho u^2}{p}\right)\frac{dp}{dx} + \frac{j'}{\omega} - \frac{\rho u^2}{\omega}\frac{d\omega}{dx}\right] \tag{A15}$$

One may substitute equation (A12) into equation (A15) to eliminate $\left(1 - \frac{1}{\gamma}\frac{\rho u^2}{p}\right)\frac{dp}{dx}$ so that

$$\frac{dp_t}{dx} = \frac{1}{2}\left(1 + b\frac{\rho u^2}{p}\right)^{\frac{1}{\gamma - 1}}\left[\left(\frac{2}{\omega} + \frac{\gamma - 1}{\gamma}\frac{\rho u^2}{p\omega}\right)j' - \frac{um'}{\omega} - \frac{\gamma - 1}{\gamma}\frac{\rho u}{p\omega}\left(q' + \frac{1}{2}u^2 m'\right)\right] \tag{A16}$$

Finally, note that

$$b\,\frac{\rho u^2}{p} = \frac{\gamma - 1}{2}\,M^2 \tag{A17}$$

so that equation (A16) becomes

$$\frac{dp_t}{dx} = \frac{1}{\omega}\left(1 + \frac{\gamma - 1}{2}\,M^2\right)^{\frac{\gamma}{\gamma-1}} j' - \frac{1}{2\omega}\left(1 + \frac{\gamma - 1}{2}\,M^2\right)^{\frac{1}{\gamma-1}}\left[um' + (\gamma - 1)M^2\left(q' + \frac{1}{2}\,u^2 m'\right)\right] \tag{A18}$$

Thus, dp_t/dx is a linear function of m', j', and q'.

Now, obtain an expression for the gradient of entropy ds/dx for steady flow. Differentiate equation (A6) to obtain

$$\frac{dh_t}{dx} = \frac{de}{dx} + p\,\frac{dv}{dx} + v\,\frac{dp}{dx} + u\,\frac{du}{dx} \tag{A19}$$

By the second law of thermodynamics, the differentials de, ds, and dv for a pure substance are related as

$$de = T\,ds - p\,dv \tag{A20}$$

Substitution of equation (A20) into equation (A19) gives

$$\frac{dh_t}{dx} + T\,\frac{ds}{dx} + v\,\frac{dp}{dx} + u\,\frac{du}{dx} \tag{A21}$$

Expressions for dh_t/dx and $u\,\frac{du}{dx} + v\,\frac{dp}{dx}$ are obtained from equations (A5) and (A9). Substitution of these expressions into equation (A21) gives

$$\frac{ds}{dx} = \frac{1}{T}\left(\frac{um' - j'}{\rho\omega} + \frac{q' - h_t m'}{\rho u \omega}\right) \tag{A22}$$

Equation (A22) may be rewritten as

$$\frac{ds}{dx} = \frac{R}{pu\omega}\left[\left(\frac{u^2}{2} - h\right)m' - uj' + q'\right] \tag{A23}$$

REFERENCES

1. Kilgore, Robert A.; Goodyer, Michael J.; Adcock, Jerry B.; and Davenport, Edwin E.: The Cryogenic Wind-Tunnel Concept for High Reynolds Number Testing. NASA TN D-7762, 1974.

2. Blanchard, A.; Dor, J. B.; and Breil, J. F.: Measurements of Temperature and Pressure Fluctuations in the T'2 Cryogenic Wind Tunnel. NASA TM-75408, 1980.

3. Fuller, Dennis E.: Guide for Users of the National Transonic Facility. NASA TM-83124, 1981.

4. Lambiotte, Jules J., Jr.; and Howser, Lona M.: Vectorization on the STAR Computer of Several Numerical Methods for a Fluid Flow Problem. NASA TN D-7545, 1974.

5. Abbott, Michael M.; and Van Ness, Hendrick C.: Schaum's Outline of Theory and Problems of Thermodynamics. McGraw-Hill Book Co., c.1972.

6. Liepmann, H. W.; and Roshko, A.: Elements of Gasdynamics. John Wiley & Sons, Inc., c.1957.

7. Carrière, Pierre: The Injector Driven Tunnel. Problems of Wind Tunnel Design and Testing, AGARD-R-600, Dec. 1973, pp. 4-1 - 4-56.

8. Allen, Theodore, Jr.; and Ditsworth, Richard L.: Fluid Mechanics. McGraw-Hill Book Co., c.1972.

9. Rao, D. M.: Wind Tunnel Design Studies and Technical Evaluation of Advanced Cargo Aircraft Concepts. Tech. Rep. 76-T11 (NASA Grant NSG 1135), Old Dominion Univ. Res. Found., May 1976. (Available as NASA CR-148149.)

10. McAdams, William H.: Heat Transmission, Third ed. McGraw-Hill Book Co., Inc., 1954.

11. Henry, John R.; Wood, Charles C.; and Wilbur, Stafford W.: Summary of Subsonic-Diffuser Data. NACA RM L56F05, 1956.

12. Shapiro, Ascher H.: The Dynamics and Thermodynamics of Compressible Fluid Flow. Volumes I and II. Ronald Press Co., c.1953 and 1954.

13. Gumas, George: The Dynamic Modelling of a Slotted Test Section. NASA CR-159069, 1979.

14. MacCormack, Robert W.: An Efficient Explicit-Implicit-Characteristic Method for Solving the Compressible Navier-Stokes Equations. Computational Fluid Dynamics, SIAM-AMS Proceedings, Volume XI, American Math. Soc., 1978, pp. 130-155.

15. Turkel, Eli: Numerical Methods for Large-Scale, Time-Dependent Partial Differential Equations. Computational Fluid Dynamics, W. Kollman, ed., Hemisphere Pub. Corp., 1980, pp. 128-262.

16. Hindmarsh, A. C.: A Collection of Software for Ordinary Differential Equations. American Nuclear Society Proceedings of the Topical Meeting on Computational Methods in Nuclear Engineering - Volume 3, Apr. 1979, pp. 8-1 - 8-15.

17. Thibodeaux, Jerry J.; and Balakrishna, S.: Development and Validation of a Hybrid-Computer Simulator for a Transonic Cryogenic Wind Tunnel. NASA TP-1695, 1980.

18. Armstrong, Ernest S.; and Tripp, John S.: An Application of Multivariable Design Techniques to the Control of the National Transonic Facility. NASA TP-1887, 1981.

1. Report No.	2. Government Accession No.	3. Recipient's Catalog No.
NASA TP-2177		

4. Title and Subtitle	5. Report Date
DEVELOPMENT OF A DISTRIBUTED-PARAMETER MATHEMATICAL MODEL FOR SIMULATION OF CRYOGENIC WIND TUNNELS	September 1983
	6. Performing Organization Code 505-31-53-09
7. Author(s) John S. Tripp	8. Performing Organization Report No. L-15591
	10. Work Unit No.
9. Performing Organization Name and Address NASA Langley Research Center Hampton, VA 23665	11. Contract or Grant No.
	13. Type of Report and Period Covered Technical Paper
12. Sponsoring Agency Name and Address National Aeronautics and Space Administration Washington, DC 20546	14. Sponsoring Agency Code

15. Supplementary Notes

16. Abstract

A one-dimensional distributed-parameter dynamic model of a cryogenic wind tunnel has been developed which accounts for internal and external heat transfer, viscous momentum losses, and slotted-test-section dynamics. Boundary conditions imposed by liquid-nitrogen injection, gas venting, and the tunnel fan have been included. A time-dependent numerical solution to the resultant set of partial differential equations has been obtained on a CDC CYBER 203 vector-processing digital computer at a usable computational rate. Preliminary computational studies were performed by using parameters of the Langley 0.3-Meter Transonic Cryogenic Tunnel. Studies have been performed by using parameters from the National Transonic Facility (NTF). The NTF wind-tunnel model has been used in the design of control loops for Mach number, total temperature, and total pressure and for determining interactions between the control loops. It has been employed in the application of optimal linear-regulator theory and eigenvalue-placement techniques to develop Mach number control laws.

17. Key Words (Suggested by Author(s))	18. Distribution Statement
Wind tunnel Transonic Cryogenic Mathematical modeling Process control	Unclassified - Unlimited Subject Category 66

19. Security Classif. (of this report)	20. Security Classif. (of this page)	21. No. of Pages	22. Price
Unclassified	Unclassified	50	A03

For sale by the National Technical Information Service, Springfield, Virginia 22161

NASA-Langley, 1983